The Dissertation Committee for Jaemin Ahn Certifies that this is approved version of the following dissertation:

All Epitaxial Mode and Current Confined Semiconductor Laser Using Selective Fermi Level Pinning

Committee:

Dennis G. Deppe, Supervisor

Dean P. Neikirk

Jack Lee

Leonard F. Register

Brian A. Korgel

All Epitaxial Mode and Current Confined Semiconductor Laser Using Selective Fermi Level Pinning

by

Jaemin Ahn, B. S.; M. S.

Dissertation

Presented to the Faculty of the Graduate School of
The University of Texas at Austin
in Partial Fulfillment
of the Requirements
for the Degree of

Doctor of Philosophy

The University of Texas at Austin
August 2005

All Epitaxial Mode and Current Confined Semiconductor Laser Using Selective Fermi Level Pinning

Publication No. ___________

Jaemin Ahn, Ph. D.
The University of Texas at Austin, 2005

Supervisor: Dennis G. Deppe

This dissertation presents a new lithographically defined approach to form self-aligned mode- and current-confined all-epitaxial GaAs-based VCSELs and quantum dot lasers. The mode confinement mechanism by intracavity phase shifting mesa is verified by a specially designed mode confined VCSEL, which shows the lasing peaks only on the phase shifting mesa with relatively low threshold current density.

The current-confining mechanism, which is self aligned with mode confining phase shifting mesa using selective Fermi-level pinning is verified with the test structure with the same active layers in the cavity by substantially increasing the turn on voltage of the region outside mesa. The mode- and current-confined VCSEL also shows improved slope efficiency and lasing spectrum which indicate the only lasing on the mesa region throughout the entire operation range.

All-epitaxial, fully planarized mode- and current-confined VCSELs, which have only single phase shifting mesa and surrounding current blocking regions are successfully demonstrated with considerably improved efficiency and threshold current density.

As an important application of this technology, all-epitaxial index- and current-confined quantum dot laser is demonstrated. The performances of quantum dot laser shows ground state lasing and stable operation up to high input current of 1.5 A. Extracted waveguide loss indicates additional loss is coming from the current blocking hetero-interfaces which can be reduced by optimization of regrowth condition.

TABLE OF CONTENTS

Chapter 1. Introduction

1.1 Technologies for Lateral Confinement of VCSELs

Vertical-Cavity Surface-Emitting Lasers (VCSELs) have been developed for more than a quarter of a century since their invention in 1978. Due to the VCSELs unique features such as beam characteristics, scalability, optoelectronic design, fabrication, and array configurability that are far more advanced compared to the traditional edge emitting laser, VCSELs are now one of the major categories of optoelectronic devices currently being manufactured.

The material system that is the most attractive to date for fabricating VCSELs is AlGaAs/GaAs because the lattice-matching is straightforward, the epitaxial growth is well-developed, and the index contrast between the AlAs and GaAs materials results in very high quality mirrors. As a result of the use of this material system, the most advanced characteristics of VCSELs, which have an active region with a strained InGaAs/GaAs or GaAs/AlGaAs quantum wells, have been produced in the 830 nm to 980 nm light emitting ranges. Moreover, the selective oxidation of AlGaAs at relatively a low temperature (~400°C) has dramatically improved the characteristics of VCSELs .

Typical VCSELs have an optical cavity of a multiple of half-wavelength thickness with an active quantum well layer and two high-reflectivity mirrors which surround the optical cavity for the longitudinal confinement of light. The mirror consists of alternating pairs of quarter wavelength thick high and low refractive index layers, composed of either monolithically grown semiconductor layers or dielectric materials deposited after epitaxial growth. Historically, three basic schemes of VCSELs have been deployed. Shown in Figure 1.1, these structures are characterized by the methods used to inject current and confine the optical mode in a lateral direction.

The first structure in Figure 1.1(a) is called the etched-post structure, where a deep mesa is etched in the layers above the region. In this type of device, the injected carriers are confined from the top contact through the upper Distributed Bragg Reflector (DBR) layers. This structure also provides optical mode confinement by a waveguide formed in the upper etched portion of the cavity. Despite the elaborate waveguide structure, for small size mesas, the optical scattering loss due to roughness of sidewalls in the etched waveguide has been identified as a major problem [1.1].

The second structure in Figure 1.1(b) is fabricated by the implantation of proton ions into the top DBR layers. When implanted into the GaAs/AlGaAs layers, the ions knock atoms off their lattice sites and create semi-insulating materials. The current aperture is formed between resistive regions. This structure has been popular due to the planar geometry of the final device, which provides low contact resistance and good thermal characteristics. However, since the implantation does not change the optical properties of material, there is no deliberate index guiding structure in the lateral direction. The lack of a well-designed index guiding mechanism results in a very high optical loss when the active volume becomes smaller than the minimum mode size of the planar cavity. The thermal lensing and self-focusing effects provide a stable mode under continuous operation with only a constant average power [1.2].

The third structure in Figure 1.1(c) is achieved by the use of a thin oxide aperture buried inside an epitaxial structure. Exposing AlGaAs alloy to temperatures ranging from 350°C to 500°C in a steam environment converts the semiconductor into a mechanically robust, chemically inert, insulating and low refractive index oxide [1.3]. The current confinement is established as the carriers are funneled through the aperture made by the insulating oxide layer. In addition to this, due to the fact that the index of the oxide layer (~1.6) is lower than that of semiconductors (~3.0), the oxide aperture provides an index guiding structure to confine the optical mode. Therefore, oxide-confined VCSELs have been shown to yield superior device performances such as a low threshold of ~10μA and a high wall plug efficiency of ~50%. This structure represents a major improvement over that of the implanted planar VCSELs, the most popular device structure currently being manufactured.

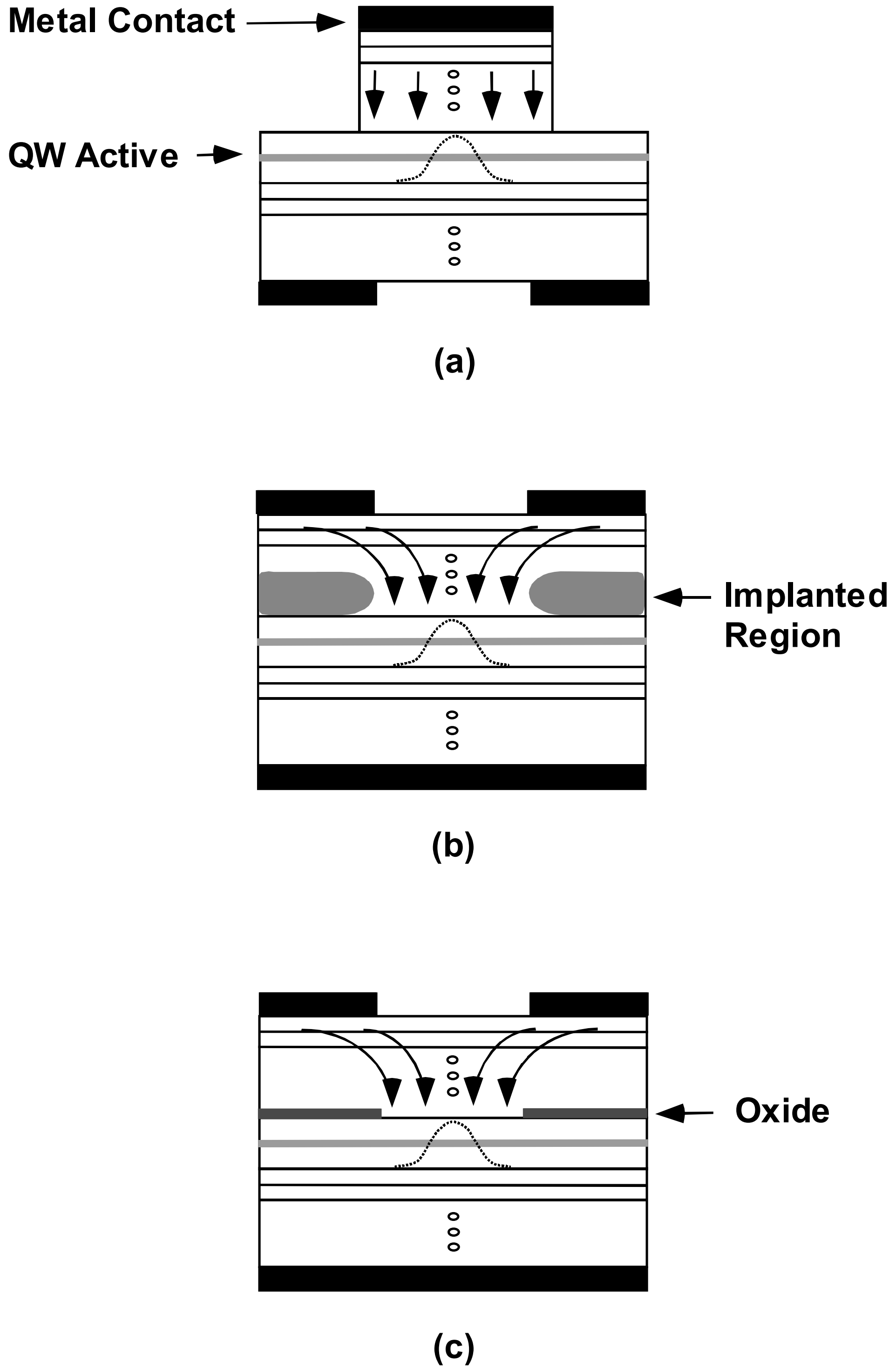

Figure 1.1 Schematics of VCSEL structures. Shown here are (a) etched post, (b) ion implanted, and (c) oxide-confined VCSELs.

1.2 Motivations of Lithographically Defined Lateral Confinement

Despite of superior performances, oxide-confined VCSELs have problems pertaining to the control, reproducibility, uniformity of oxidation and reliability. Because the oxide aperture is formed from a diffusion process and because it has a different thermal expansion coefficient than the semiconductor, it can produce problems with regard to reproducibility and reliability. There are several studies on the defects that are near the oxide/semiconductor interface induced by the oxidation process [1.4]. The strain fields of the defects may affect device performance when the active layer is near the oxide interface [1.5]. Moreover, the oxidation process functions differently in circular mesas than in strips and has a unique time- and crystallographic dependence in square mesas [1.6]. These problems become more serious for small area and single mode VCSELs.

Another approach to mode- and current-confinement has been to use shallow mesas with non-epitaxial mirrors, sometimes using implantation or tunnel junctions for current-confinement [1.7], [1.8]. However, the tunnel junction/mesa approach yields an undesirable mesa step and additional voltage drop when used in GaAs-based VCSEL. In addition, dielectric mirrors can introduce material strain, complicate device fabrication, and degrade reliability. As a result, an effective means has not yet been demonstrated to reproducibly fabricate all-epitaxial GaAs-based VCSELs that simultaneously obtain both current-confinement and mode-confinement to eliminate thermal lensing effects and achieve a low threshold.

In this work, I will demonstrate a new lithographically defined approach to form self-aligned mode- and current-confined all-epitaxial GaAs-based VCSELs. This new process is based on epitaxial regrowth over an intracavity phase-shifting mesa. The device is illustrated in Figure 1.2. An intracavity phase-shifting mesa is lithographically patterned and selectively etched on the first part of the VCSEL, which comprises the bottom DBR and single wave-length cavity. As one of the important applications, I demonstrate all-epitaxial index- and current-confined quantum dot lasers using the same process and growth technology. This technology has the following advantages over the conventional lateral confinement methods. The lithographically defined aperture can provide excellent uniformity and manufacturability down to the nanometer scale. The lithographic patterning provides flexibility of aperture design such as dense 2-D arrays, nano-scale grating, and arbitrary shape. Finally, all-semiconductor epitaxial VCSELs can give higher long-term reliability with the elimination of internal strain due to wet oxidation.

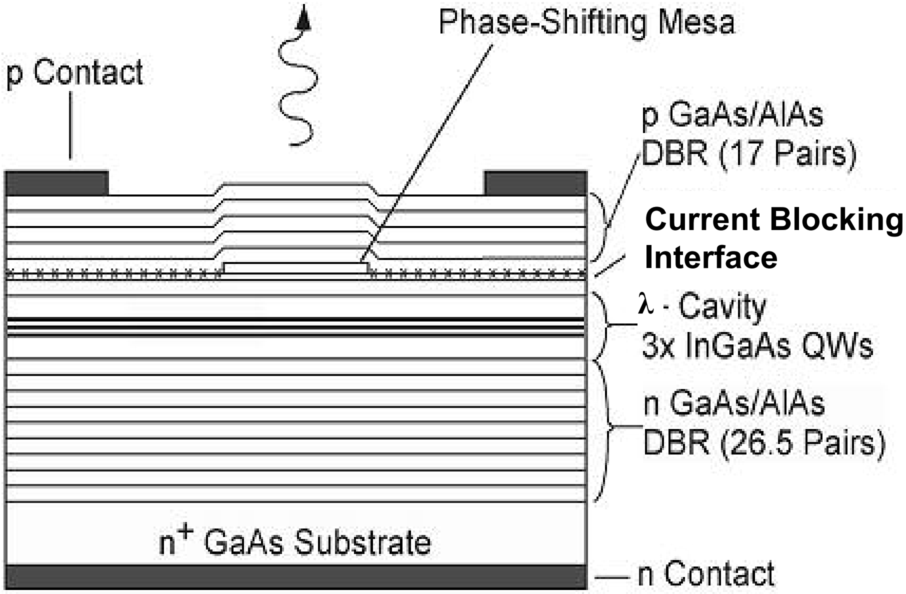

Figure 1.2 Schematic of all Epitaxial lithographically defined mode- and current confined VCSEL

1.3 Outline

This dissertation addresses the importance of all-epitaxial and lithographic approach in the semiconductor laser. The mode-confinement mechanism and simultaneous current-confinement mechanism for all-epitaxial mode-and current-confined semiconductor lasers are proposed and verified. Using these technologies, the all-epitaxial mode- and current-confined VCSEL is demonstrated. Finally, as one of the important applications, all-epitaxial mode- and current-confined quantum dot laser is demonstrated with the same technologies.

In Chapter 1, the background of this work and the basic knowledge of the lateral confinement technology for VCSEL are discussed. The motivations of the all-epitaxial approach are also discussed. In addition, the outline of this dissertation is presented in order to introduce the overall ideas of this research.

In Chapter 2, the lateral mode-confinement mechanism of the VCSEL by the phase-shifting intracavity mesa is proposed. The mode-confinement mechanism is verified by a specially designed mode-confined VCSEL, which does not have any current-confinement on the phase-shifting mesas.

All-epitaxial mode- and current-confined VCSELs are demonstrated in Chapter 3 and Chapter 4. The current-confining mesa, which is self-aligned with mode-confining phase-shifting mesa using selective Fermi-level pinning, is proposed and verified by the VCSEL with a similar structure to mode-confined VCSEL in Chapter 3.

All-epitaxial, fully planarized mode- and current-confined VCSELs, which have only a single phase-shifting mesa and surrounding current blocking region are demonstrated in Chapter 4. The effect of the current blocking interface on the performances is discussed.

Chapter 5 is focused on the all- epitaxial index- and current-confined quantum dot laser using the same patterning technology and the current-confining mechanism with VCSELs. Performances of quantum dot lasers are presented and the waveguide losses are analyzed

In Chapter 6, the conclusion of this research is summarized and future research topics are proposed.

1.4 References

[1.1] B.J. Thibeault, T.A. Strand, T. Wipiejewski, M.G. Peters, D.B. Young, S.W. Corzine, L.A. Coldren, and J.W. Scott, "Evaluating the effect of optical and carrier lossed in etched post vertical cavity lasers," *J. Appl. Phys.* Vol.78, pp. 5871-5875, 1995

[1.2] K.L. Lear, R.P. Schneider, Jr. K.D. Choquette, and S.P. Kilcoyne, "Index guiding effects in implant and oxide confined vertical-cavity lasers," *IEEE Photon. Technol. Lett.*, Vol. 8, pp. 740-721, 1996

[1.3] N. Holonyak, Jr., and J.M. Dallesasse, USA Patent #5,262,360 , 1993

[1.4] S. Guha, F. Agahi, B. Pezeshki, J.A. Kash, D.W. Kisker, and N.A. Bojarczuk, "Microstructure of AlGaAs-oxide heterolayers formed by wet oxidation," *Appl. Phys. Lett.*, Vol. 68, pp. 906-908, 1996

[1.5] A.C. Alonzo, X.C. Cheng, and T.C. McGill, "Strain in wet thermally oxidized square and circular mesas," *J. Appl. Phys.* Vol.87, pp. 4594-4599, 2000

[1.6] J.P. Landesman, A. Fiore, J. Nagle, V. Berger, E. Rosencher, and P. Puech, "Local stress measurements in laterally oxidized GaAs/AlGaAs heterostructures by micro-Raman spectroscopy," *Appl. Phys. Lett.*, Vol. 71, pp. 2520-2522, 1996

[1.7] L.M.F. Chirovsky, W.S. Hobson, R.E. Leibenguth, S.P. Hui, J. Lopata, G.J. Zydik, G. Giaretta, K.W. Goosen, J.D. Wynn, A.V. Krishnamoorthy, B.J. Tseng, J.M. Vandenberg, and L.A. D'Asaro, "Implant-apertured and index-guided vertical-cavity surface-emitting lasers (I2-VCSELs)," *IEEE Phot. Tech. Lett.*, Vol. 11, pp. 500-502, 1999

[1.8] M. Ortsiefer, R. Shau, G. Bohm, F. Kohler, and M.-C. Amann, "Low-threshold index guided 1.5 μm long-wavelength vertical-cavity surface-emitting laser with high efficiency," *Appl. Phys. Lett.*, Vol. 76, pp. 2179-2181, 2000

Chapter 2. Mode Confinement of VCSEL by Intracavity Phase Shifting Mesa

2.1 Diffraction Loss and Scattering Loss of VCSELs

Mode confinement mechanism in a VCSELs structure with phase-shifting mesas can be explained with the same model for VCSELs with dielectric apertures [2.1]. An idealized Fabry-Perot microcavity is formed by two perfect mirrors with 100% reflectivity as shown Figure 2.1. The cavity between mirrors is divided by into two regions by step height as illustrated in Figure. The region “0” with r < w/2 is the lasing region where the lasing eigenmode exists. This region has the cavity length, which is tuned for a specific resonance wavelength. The region “1” with r > W/2 is the waveguide region and extends to infinity in lateral direction. This region also has the cavity length, which is tuned for another specific resonance wavelength.

Due to the reflection at the mirrors, standing wave interference patterns are formed in the direction normal to the mirrors, and the tangential electric field must vanish at each mirror interface. These standing wave patterns will allow only certain discrete values for the z component of wavevector in region “0” and “1”. These vertical wavevector are given by

$$k_{z,0} = \pi m_z / \sqrt{\varepsilon} L_0 \qquad (2.1)$$

in region “0”, and

$$k_{z,1} = \pi m_z / \sqrt{\varepsilon} L_1 \tag{2.2}$$

in region "1", where ε is the relative permittivity in the cavity, L_0 is the effective cavity length in region "0", L_1 is the effective cavity length in region "1", and m_z can be a zero or positive integer, i.e. m_z=0,1,2,... This restriction on the vertical wavevectors will change the waveguide mode density in region "1".

For a cylindrically symmetric aperture, the lowest order eigenmode confined by aperture region "1" takes its field profile the form of a Bessel function of first kind for r< w/2. Considering the lowest order eigenmode as having a frequency of ω_o, it will overlap the mode density of cladding region "1", under the condition of

$$\frac{\omega_o}{c} = \sqrt{\frac{(4.810)^2}{\varepsilon \cdot w^2} + k_{z,0}^2} = \sqrt{k_{\rho,1}^2 + k_{z,1}^2} \tag{2.3}$$

where the optical mode size, w and $k_{z,0} = \pi m_z / \sqrt{\varepsilon} L_0$ satisfies the vertical resonance condition in region (a), and the factor 4.810 comes from the cylindrical symmetry and the assumption of a Bessel function solution. With the equivalent m_z values in both regions, following relation is obtained between the vertical wavevectors in two regions form equations (2.1) and (2.2)

$$k_{z,0}^2 < k_{z,1}^2 \tag{2.4}$$

Therefore, there exists a range of mode sizes *w* for $k_{\rho,1}^2$ <0, which meaning that $k_{\rho,1}$ is imaginary and the mode is confined in region "0".

While the phase-shift effectively eliminates diffraction loss in the otherwise planar cavity, it does so at the penalty of introducing scattering loss due to the nonorthogonality of the longitudinal modes between regions "0" and "1" as shown in

Figure 2.2. This scattering is characterized by the normalized overlap of the longitudinal resonant field E_0(z) in cavity region "0" with the longitudinal resonant field E_1(z) in cavity region "1," given by

$$|C|^2 = \frac{\left|\int E_0^*(z) \cdot E_1(z)dz\right|^2}{\int E_0^*(z) \cdot E_0(z)dz \cdot \int E_1^*(z) \cdot E_1(z)dz} \tag{2.5}$$

where, $|C|^2 \leq 1$. When the phase-shifting mesa height goes to zero, $|C|^2 = 1$, and scattering is eliminated at the penalty of increasing diffraction loss due to a decreasing lateral mode size. Oxide-confined VCSELs are rather unique in that $|C|^2$ can be near unity because of nearly perfect overlap in the longitudinal fields between the unoxidized and oxidized regions, effectively eliminating both diffraction and scattering losses relative to transmission loss through the mirrors. From the calculation, it is found that the step height of intracavity phase shifting mesa, which is placed at the 1st node in upper DBR has strong adverse effect on the scattering loss factor, $|C|^2$, as increasing the step height. To achieve the same effects in the all-epitaxial VCSEL the phase shifting layer in Figure. 2.2 must barely disrupt the longitudinal field profiles between regions "0" and "1."

It is clear that this all-epitaxial approach can produce mode-confinement very similar to the oxide-confined VCSEL. Equations (2.3) and (2.5) provide a direct comparison between the all-epitaxial design based on a phase-shifting mesa and that due to oxide-confinement. Both the oxide confinement and the all-epitaxial designs depend on the precise placement of the oxide or phase-shifting mesa, as well as the oxide-thickness or mesa height. However, considering both equations (3) and (5) presents some surprises over conventional thinking about oxide-aperture loss [2.4],[2.5]. Given the same mode confinement, the lowest optical loss for either the oxide or the phase-shifting mesa occurs when either are placed at an anti-node in the cavity, since much thinner layers can then be used to obtain the same mode confinement and thinner layers disrupt the longitudinal resonant fields between regions "0" and "1" less ($|C|^2$ becomes closer to unity). However, very thin oxide layers are difficult to fabricate, and oxide thicknesses of 100 Å or greater provide more than sufficient mode confinement even when placed at nodes.

To illustrate a direct comparison, a 980 nm oxide confined VCSEL based on AlAs/GaAs reflectors with a 463 Å oxide layer placed at the first node of the upper mirror results in a 40 Å resonance shift, giving a minimum optical mode size from equation (2.3) of 2.5 mm, with a scattering parameter from equation (2.5) of $|C|^2 = 0.990$. To obtain the same mode confinement with the all-epitaxial approach, the phase shifting mesa is also placed at the first node of the upper mirror, has a height of 66 Å to create the 40 Å resonance shift, and gives a scattering parameter of $|C|^2 = 0.994$. Therefore the all-epitaxial approach based on the phase-shifting mesa represents a scheme that can outperform the oxide confined VCSEL for low loss mode confinement.

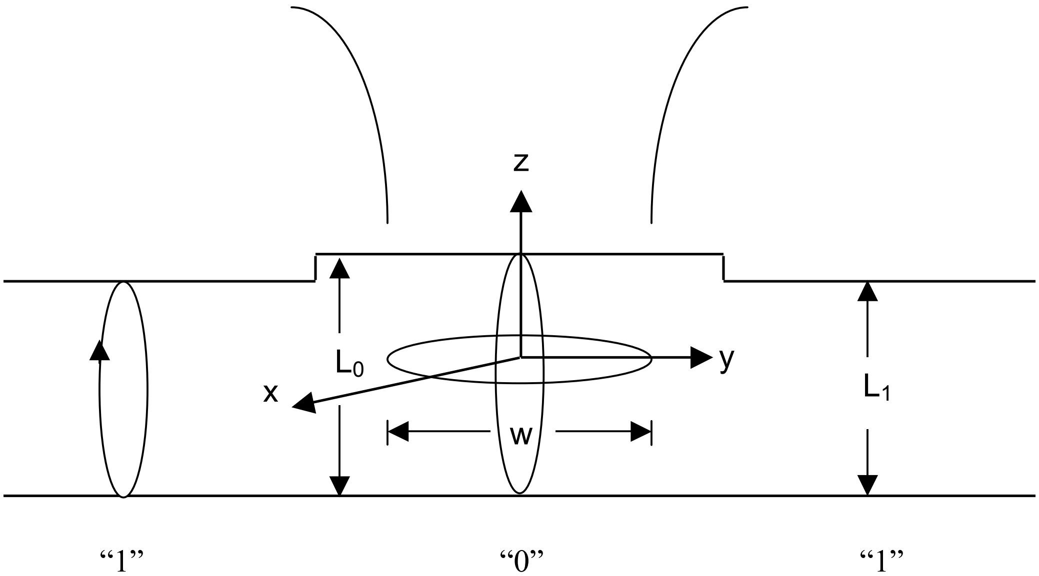

Figure 2.1 Schematic illustration of the idealized Fabry-Perot microcavity with a phase shifting mesa. The region "0" has a lasing eigenmode and the region "1" has waveguiding modes.

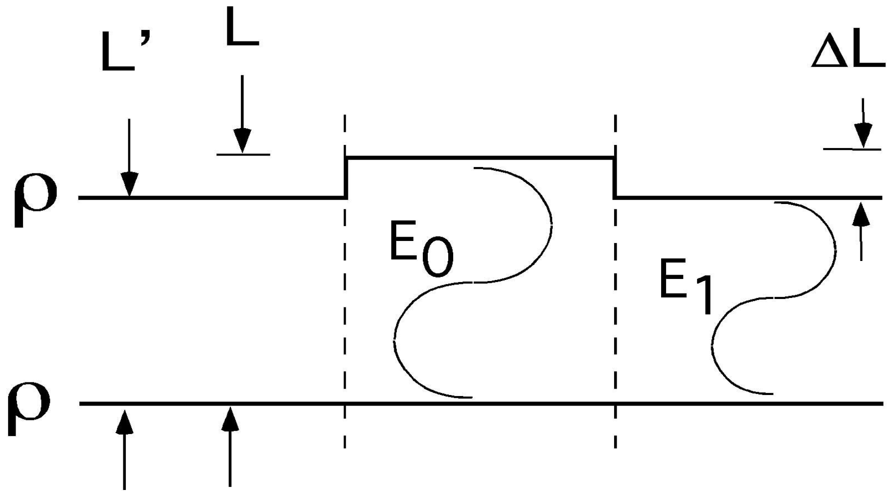

Figure 2.2 Schematic illustration of in the idealized Fabry-Perot microcavity with a phase shifting mesa. E_0 is the longitudinal resonant field in the region "0", E_1 is the longitudinal resonant field in the region "1"

2.3 Verification of Mode Confinement by Phase Shifting Mesa

Mode confinement by phase shifting mesa is verified by a specially designed mode confined VCSEL, which does not have any current confinement on the phase shifting mesas. The current is funnel into the region including phase shifting mesa and surrounding waveguide region by outer aperture, which blocks the current using back biased p-n junction.

2.3.1 Design and structure of mode confined VCSEL

Figure 2.3(a) shows a schematic illustration of the VCSEL presented. It is based on an intracavity phase-shifting layer placed in a fully epitaxial cavity. The phase-shifting layer eliminates the need for oxide to achieve mode confinement. I find that both the placement and height of the phase shifting mesa as shown in region “0” of Figure 2.3(a) must be carefully designed to achieve low optical loss. I note that an effective index model considers only the shift in the vertical resonances between regions “0” and “1” in its analysis, and is not very useful for high quality VCSEL design because of the importance of optical loss.

Figure 2.3(b) shows an optical photograph looking down at the surface of an all-epitaxial VCSEL that contains a phase-shifting intracavity mesa and current aperture as shown in Figure 2.3(a). The phase-shifting mesa is 7 μm diameter and only 125 Å in height, and cannot be seen in the optical photograph of Figure 2.3(b). The phase-shifting mesa is placed within a current confining aperture of 15 μm diameter formed from back biased p-n junctions. A boundary exists between the phase-shifting mesa and the current confining aperture to limit scattering of the lasing mode. Although additional electrical confinement may be implemented to confine the current solely to the 7 μm diameter phase-shifting mesa, in this study current is passed through the region outside the phase-shifting mesa and within the current aperture to elucidate the optical confinement.

2.3.2 Experimental procedures

The VCSEL includes a lower *n*-type AlAs/GaAs reflector of 26.5 pairs, a wavelength thick $Al_{0.05}Ga_{0.95}As$ cavity spacer with three GaAs/InGaAs quantum wells placed at its center, and an upper 24 pair $Al_{0.7}Ga_{0.3}As$/GaAs reflector doped *p*-type with Be. As mentioned earlier, the phase shifting mesa and current funneling p-n junction is patterned before the growth of upper mirrors. Back biased p-n junction comprises a 4 $\times 10^{18}$ cm^{-3} Si doped GaAs of 800 Å and a 2 $\times 10^{18}$ cm^{-3} Be doped $Al_{0.7}Ga_{0.3}As$ of 200 Å. The process to form intracavity structure includes lithographic definition of ring pattern and selective wet etching with sacrificial layer, which ensure a free of surface contamination by photo resist as shown in Figure 2.4.

Selective wet etching is critical process for uniform and controllable intracavity structure. Because the mode confinement is governed by the mesa height, it should be thin and constant across the wafer to have uniform mode confinement and minimize the scattering loss. A GaAs of 75 Å and an $Al_{0.7}Ga_{0.3}As$ of 50 Å are used as a mesa layer. GaAs can be etched by the citric acid mixed with hydrogen peroxide by 5:1 with sufficient selectivity on $Al_{0.7}Ga_{0.3}As$ layer. $Al_{0.7}Ga_{0.3}As$ can be etched by HF (49%) diluted with water by 1:20 which does not attack GaAs layer. This selective etching process is well controlled by careful inspection and measurement of step height after every etching step.

First step is to define a ring opening pattern with photo lithography process. After masking, the top three layers, which is GaAs, $Al_{0.7}Ga_{0.3}As$, and GaAs is etched by selective wet etching, respectively. After removing photo resist, put the sample into the oxygen plasma for 5 min to remove any organic residues on the surface. Second photo lithography process is following to cover outside region and open the only inside mesa region. Second selective wet etching is performed to remove GaAs layer in the mesa region. After removing photo resist and organic residue again, selective etching of $Al_{0.7}Ga_{0.3}As$ layers in the mesa region and ring region is done simultaneously. Finally, GaAs and $Al_{0.7}Ga_{0.3}As$ layers in all three regions are etched by selective wet etching, consecutively.

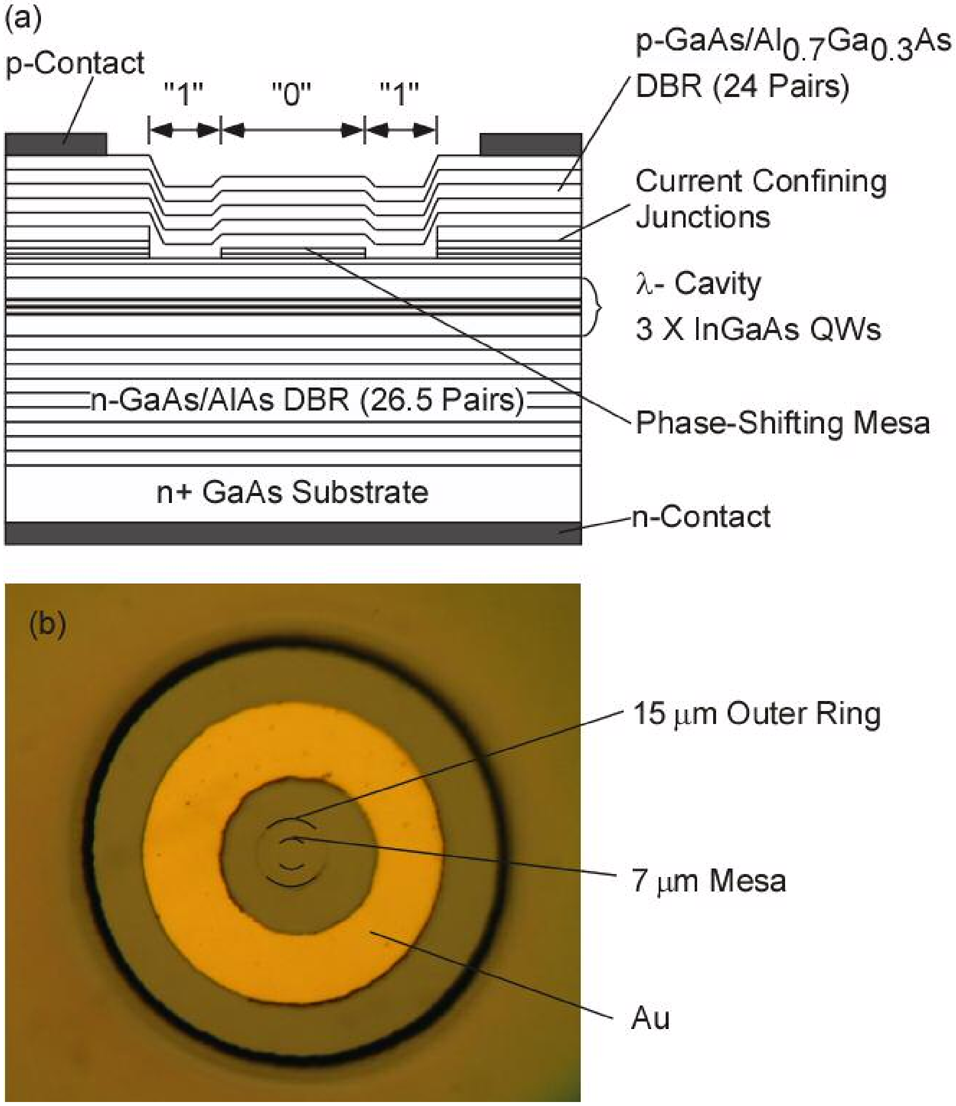

Figure 2.3 (a) A schematic illustration of the all-epitaxial VCSEL that uses an intracavity phase-shifting mesa. (b) A photograph looking down at the surface of such a VCSEL containing a 7 μm-diameter phase-shifting mesa region, and a 15 μm-diameter electrical confinement region.

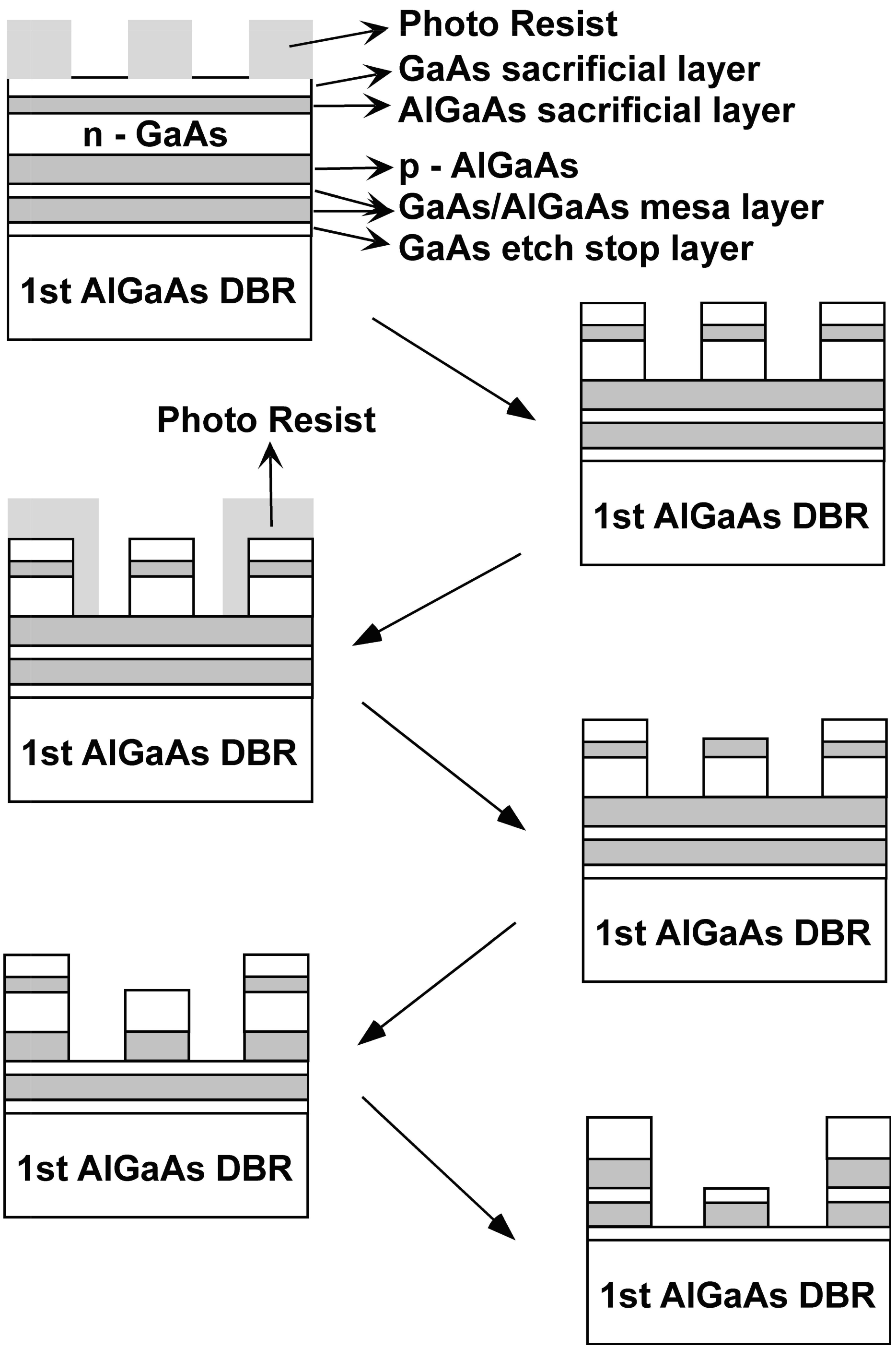

Figure 2.4 Process flow for patterning self aligned intracavity phase shifting mesa and current funneling aperture.

2.3.3 Characteristics of all epitaxial mode confined VCSELs

The mode confinement can be verified by characterizing the emission spectrum under and above the threshold current and light output versus input current of the VCSEL. Once the input current density reaches the threshold point, it can lase with the mode confinement even with some current leakage.

First, the current blocking on the back biased p-n junction and current conduction through the device is confirmed by measuring I-V characteristics of each region as shown in Figure 2.5. Ring contact with 30 μm inner diameter and 60 μm outer diameter is formed on VCSEL and 100 μm diameter pillar is etched for isolation. Turn on voltage of the device is 1.2 V, which is normal value for InGaAs QW laser while the region with back-biased p-n junction have substantially increase turn on voltage of 6.8 V, which meaning most of the injected current funnel into 15 μm-diameter aperture. Therefore the current density injected into the phase shifting mesa can be sufficiently high enough to get threshold current density.

The continuous-wave light versus current curve is shown in Figure 2.6. The threshold current of 1.3mA corresponds to a threshold current density of only 736 A/cm^2 in the total 15μm-diameter region. This low threshold current density is obtained even with a non-optimized upper $Al_{0.7}Ga_{0.3}As$/GaAs mirror chosen due to the use of Be p-doping. Despite the current injection into the entire 15μm -diam region, only the 7μm mesa region comes to threshold at 1.3mA. Assuming uniform current injection in the 15 mm region places the threshold current of the 7μm mesa region at 283μA, consistent with an oxide confined VCSEL of similar size [2.2], [2.3].

Figure 2.7 is designed resonance wavelength of phase shifting mesa region, ring shaped waveguiding region, and current blocking p-n junction region. The resonance wavelength of mesa region was designed at 980 nm, ring shaped waveguide region has resonance wavelength of 973 nm due to the effective cavity length difference comes from the mesa height of 125 Å.

Figure 2.8(a) shows the below threshold emission from both the 7 μm mesa region and the region bound by the 15μm-diameter current aperture. The transverse modes of the 7 μm phase-shifting mesa are clearly observed starting at, 972 nm with 1 nm mode spacing. The emission from the outer region bound by the 15 μm -diameter current aperture and the 7 μm diameter phase-shifting mesa can also be observed, and this emission starting at 965 nm is blue shifted with respect to that of the 7μm -diam phase-shifting mesa according to the resonance wavelength shift. The spacing between two regions is 6.84 nm which is almost same as expected from the calculation. This result shows that mode confinement is not setup by the phase shifting mesa below threshold due to the random orientation of wave vector.

As increasing current injection, lasing spectrum is obtained as shown in Fig. 2.8(b), lasing in the 7 μm mesa region occur multimode, just as with an oxide-confined VCSEL, due to the low optical loss for higher order modes. Lasing occurs over the wavelength range of 969–972 nm, and this entire spectral range lase due to a slight blue shifted detuning of the gain away from the lowest order mesa mode. This results can confirmed the mode confinement by phase shifting mesa occur once the threshold current density is reached and wave vectors are aligned to vertical. The model for mode confinement is verified.

Above 5mA, lasing also occurs in the outer ring between the 7 μm mesa and 15 μm current aperture as shown in Figure 2.9. This is due to the injected current outside the mesa which is also reached to the threshold current density of the higher order mode of the ring region. The results indicate that current confinement into the phase shifting mesa is required for stable operation of the VCSEL.

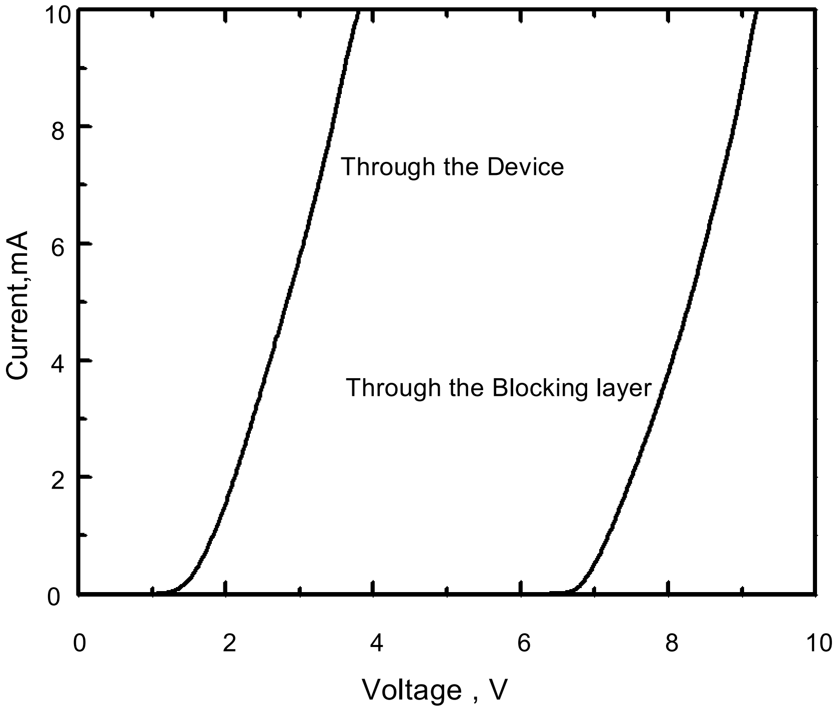

Figure 2.5 I-V characteristics of all epitaxial mode-confined 15 μm-diameter VCSEL with the 7 μm-diameter mode confining mesa region and through the back biased p-n junction region.

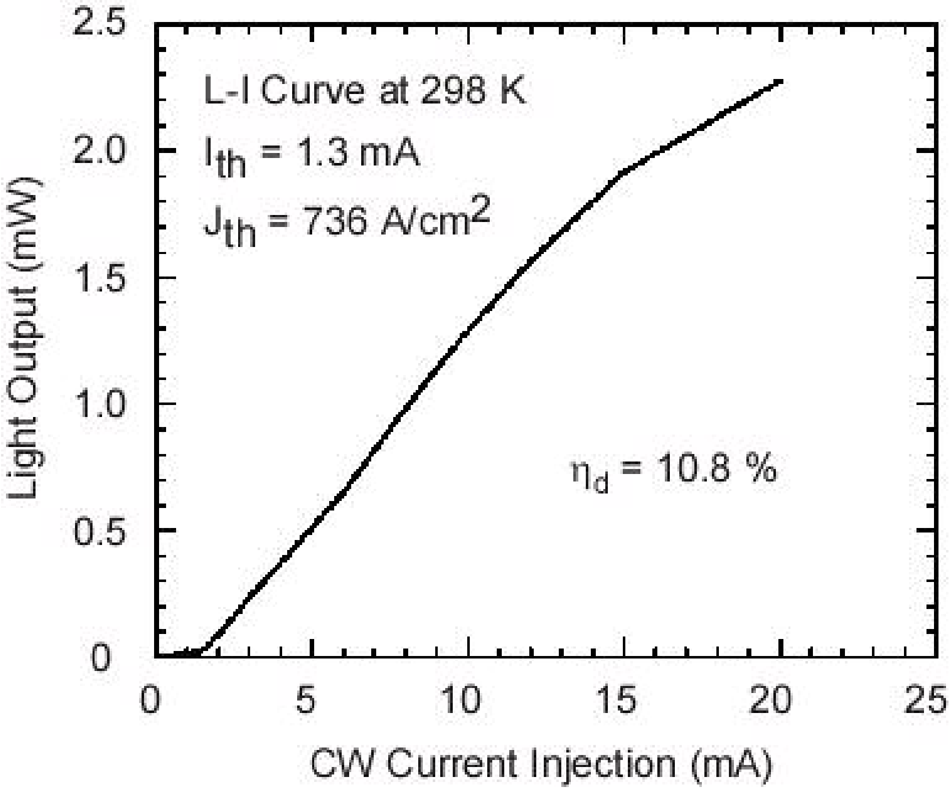

Figure 2.6 Light vs current characteristics measured for the 15 μm-diameter VCSEL of Figure 2.1. The threshold current density is only 736 A/cm^2, and lasing occurs in the 7 μm-diameter mode confining mesa region. The slope efficiency is low because of current spreading and a nonoptimized upper DBR.

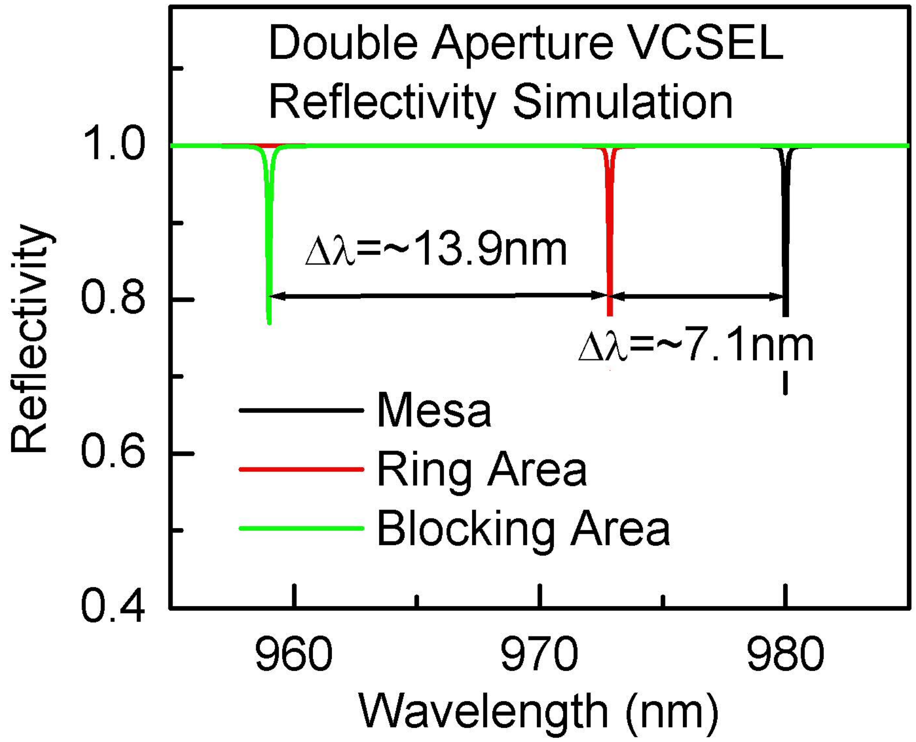

Figure 2.7 Calculated resonance wavelengths of 980 nm, 972.9 nm, and 959 nm for the phase shifting mesa region, ring shaped waveguiding region, and current blocking back- biased p-n junction region respectively.

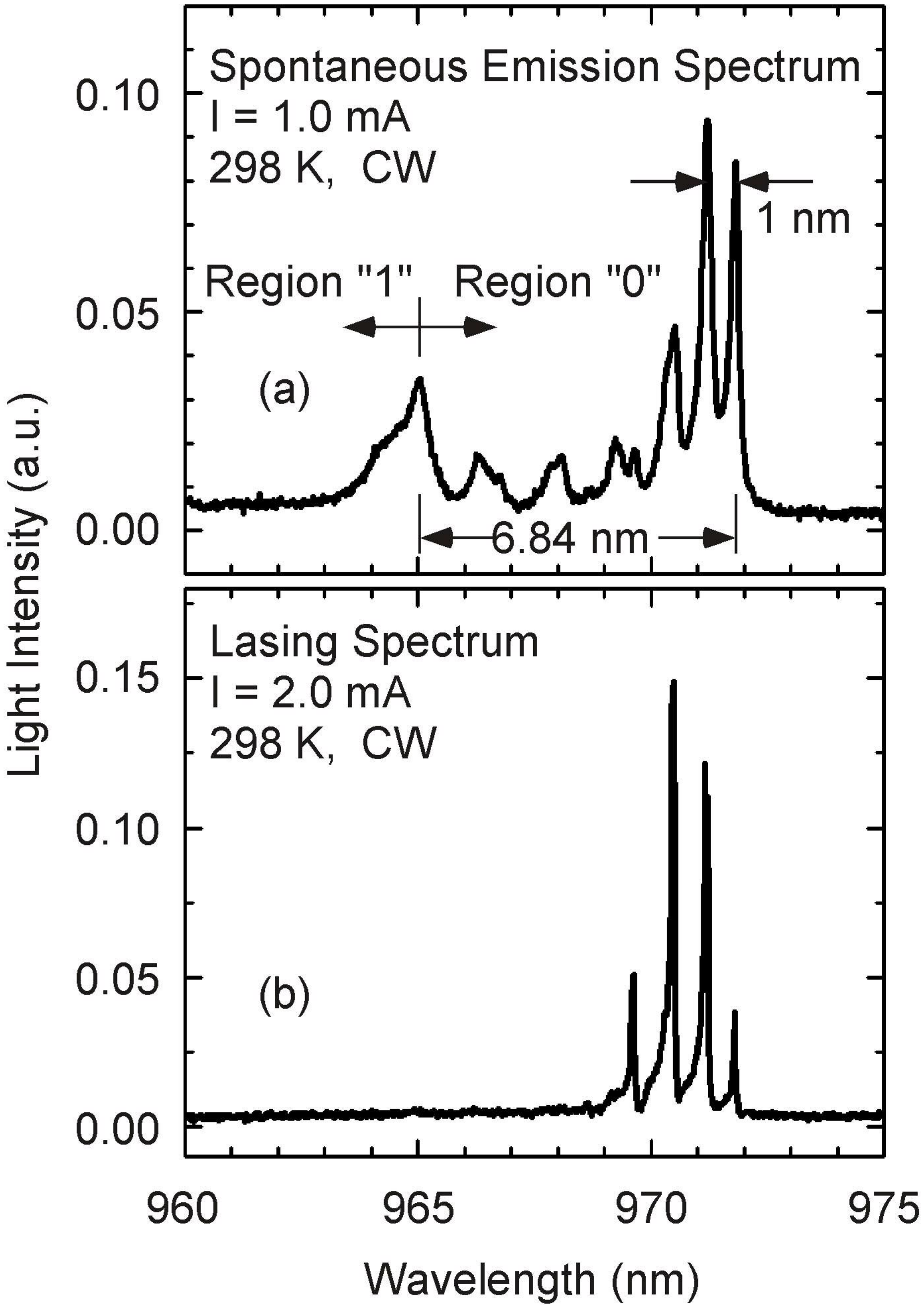

Figure 2.8 Spectral emissions both (a) just below threshold at a current density of 566 A/cm^2, and (b) just above threshold at a current density of 1.13 kA/cm^2. The spectral modes observed at wavelengths longer than 965 nm are due to the 7 μm mesa of Figure 2.1(b), or region “0” in Figure 2.1(a).

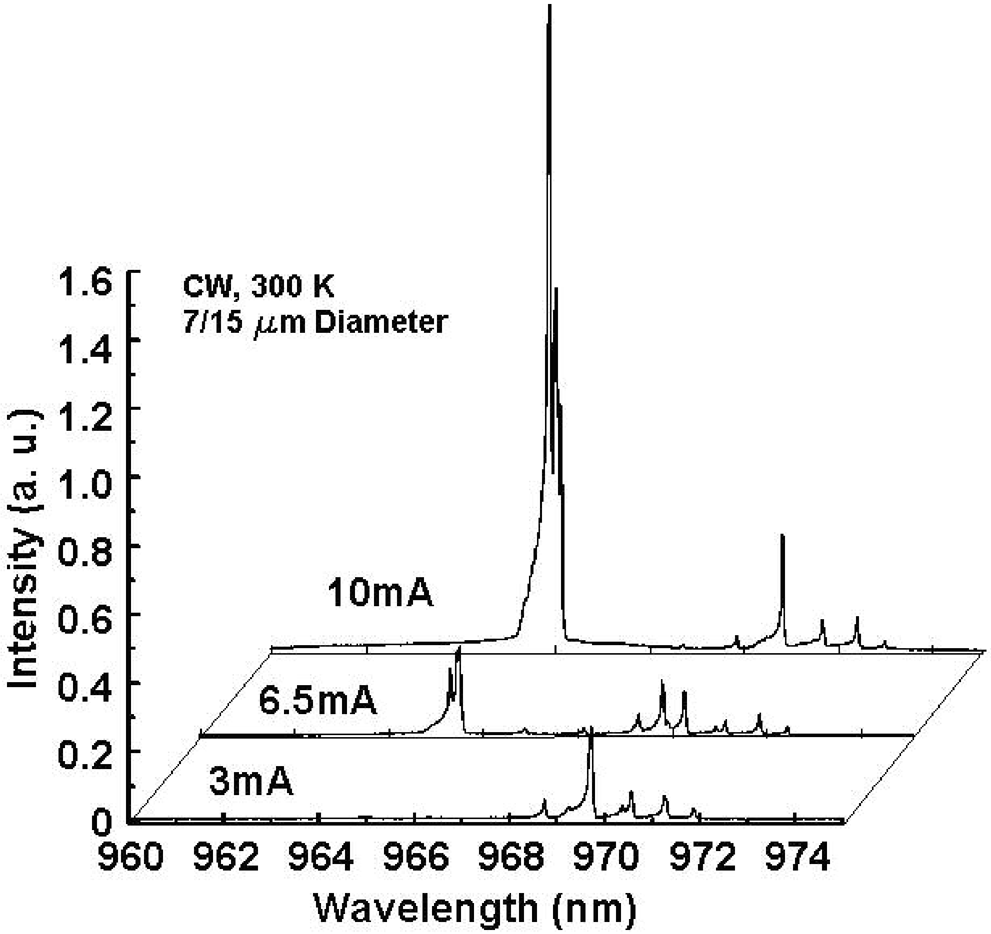

Figure 2.9 Lasing spectrum of all epitaxial mode confined VCSEL with 7 μm mesa and 15 μm current aperture at different current injection. Above 5 mA, lasing also occurs in the outer ring between the 7 μm mesa and 15 μm current aperture

2.4 Summary

Method of mode confinement by phase shifting mesa is presented and verified by the demonstration of an all-epitaxial mode confined VCSEL with several advantages in its mode confinement. These include a lithographically defined mode-confining region that can be readily extended to include intracavity two dimensional patterns such as gratings or photonic crystals, and that is reproducible even for scaling to very small sizes. The all-epitaxial approach eliminates strain by eliminating the need for oxide to achieve mode confinement, and with the potential for higher reliability as well as high reproducible manufacturing. Current confinement is introduced here due to an outer aperture based on back-biased p-n junctions, while additional techniques can be used to confine the current only to the mesa that will be described on the next chapter. Here I show the important design parameters to achieve low optical loss, and demonstrate an all-epitaxial VCSEL design to achieve this.

2.5 References

[2.1] D. G. Deppe, T.-H. Oh, and D.L. Huffaker, “Eigenmode confinement in the dielectrically apertured Fabry-Perot microcavity,” *IEEE Photonics Technol. Lett.,* Vol. 9, pp. 713-715, 1997

[2.2] D. G. Deppe, D. L. Huffaker, C. C. Lin, and T. J. Rogers, *Conference on Lasers and Electro-Optics 1994,* Technical Digest Series Vol. 8, Anaheim, CA, 8–13 May 1994, pp. CPD2-113-6/8.

[2.3] D. L. Huffaker, D. G. Deppe, K. Kumar, and T. J. Rogers, “Native-oxide defined ring contact for low threshold vertical cavity lasers,” *Appl. Phys. Lett.*, Vol. 65, pp. 97-99, 1994

[2.4] A. E. Bond, P. D. Dapkus, and J. D. O’Brien, “Aperture dependent loss analysis in vertical-cavity surface-emitting lasers,” *IEEE Photonics Technol. Lett.,* Vol. 11, pp. 397-399, 1999

[2.5] A. E. Bond, P. D. Dapkus, and J. D. O’Brien, “Aperture placement effects in oxide-defined vertical-cavity surface-emitting lasers,” *IEEE Photonics Technol. Lett.*, Vol. 10, pp. 1362-1365, 1998

Chapter 3. Current Confinement by Selective Fermi Level Pinning

3.1 Introduction

While phase shifting mesa can effectively confine the mode without any current confinement into the mesa, in order to achieve get stable operation at higher input current, better efficiency, and lower threshold current it is required to confine the current into the same intracavity mesa. The current ratio between mesa and ring region is radius squared in creasing as radius increases. Therefore this current ration should be minimizes for the large area high power VCSEL application.

In this chapter, the method to get simultaneous mode and current confinement on the phase shifting mesa with Fermi level pinning effect on the hetero-interfaces is proposed. Process issues and current confinement test is described. In order to verify current confinement, all epitaxial mode and current confined VCSEL is designed and characterized by the similar structure with the mode confined VCSEL [3.1].

3.2 Self-Aligned Current Confinement by Selective Fermi Level Pinning

The current confinement is achieved through the current blocking on the waveguide regions. Fermi level pinning phenomena are well known effect at the metal–GaAs Schottky contact. Ambient exposed GaAs contains native oxide on the surface and this oxygen can create interface state in the band gap of GaAs which leads the Fermi level at the interface is pinned at the middle of band gap regardless of doping level. Therefore metal-GaAs contact can be Schottky regardless of work function adjustment between metal and GaAs.

The similar phenomena can be occurred during the regrowth of GaAs on the AlGaAs layer. Surface native oxide on the GaAs layer is usually removed by thermal desorption at high temperature in As_4 ambient. Therefore the regrown materials follow the crystal structure of the substrate and maintain a good quality of crystal. However, the native oxide on the AlGaAs layer can not be totally removed by thermal desorption before the growth depending on the composition of Al contents. Therefore regrown interfaces are not perfect and create some defect states at the interface, which is different from the bulk Fermi level depending on dopant type and doping level. This Fermi level pinned at the middle of the bandgap and work as a Schottky barrier for carrier conduction as shown in Figure 3.1.

Using this effect, the current confinement on the intracavity phase shifting mesa of VCSELs is achieved. The intracavity mesa shown as Figure 3.2 is same mesa for the mode confinement shown in Figure 2.1. The only difference is the semiconductor layers constitute the aperture. Current confined intracavity mesa has single GaAs layer on top of $Al_{0.3}Ga_{0.7}As$ etch stop layer, which can be defined photolithography and selective etching process. As growing the GaAs layer on top of this structure, two different kinds of interface are formed. GaAs/GaAs interface might have free of interface states and Fermi level pinning effect, but GaAs/ $Al_{0.3}Ga_{0.7}As$ interface might have some interface states which leads to Fermi level pinning due to oxygen.

The process to fabricate single GaAs intracavity mesa is quite similar to the previous process for mode confined VCSEL. The only difference is the etching solution for appropriate etch stop layer. The process flow is shown in Figure 3.3. The $Al_{0.3}Ga_{0.7}As$ final etch stop layer, which works as Fermi level pinning interface should not be etched by citric acid and fluoric acid. There is range of ratio of citric acid to hydrogen peroxide gives selectivity between GaAs and $Al_{0.3}Ga_{0.7}As$ [3.2], [3.3]. In this experiment, 2:1 to 3:1 ratio gives sufficient selectivity between them.

Figure 3.4 shows the current vs. voltage characteristics measured through test structures consisting of epitaxial regrowth on either (a) the phase-shifting mesa region, or on (b) the $Al_{0.3}Ga_{0.7}As$ outside the phase-shifting mesa region. The test structures contain the same p-n InGaAs/GaAs quantum well heterostructure spacer layer as the VCSEL. The current paths in either case are constrained to 60µm diameter mesas with 30µm diameter p-side metal contacts. The measurements show that the turn-on voltage is increased from ~1.2 V in the phase-shifting mesa region to ~4.5 V in the region that would be outside the phase-shifting mesa region. This change in voltage drop is sufficient to provide excellent current confinement to the VCSEL active area. The current ratio of the test structure on the mesa to off the mesa at 1.6 V, the voltage drop at threshold, is more than 100,000. This means almost all of the injected current would flow into the phase shifting mesa selectively and simultaneous mode and current confinement can be achieved.

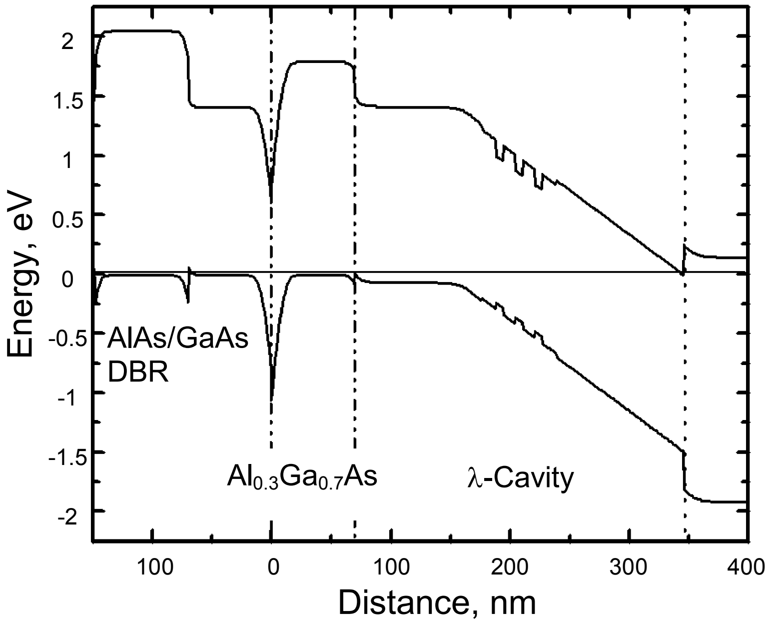

Figure 3.1 Energy band diagram of VCSEL near the cavity including Fermi level pinning effect at GaAs/AlGaAs interface.

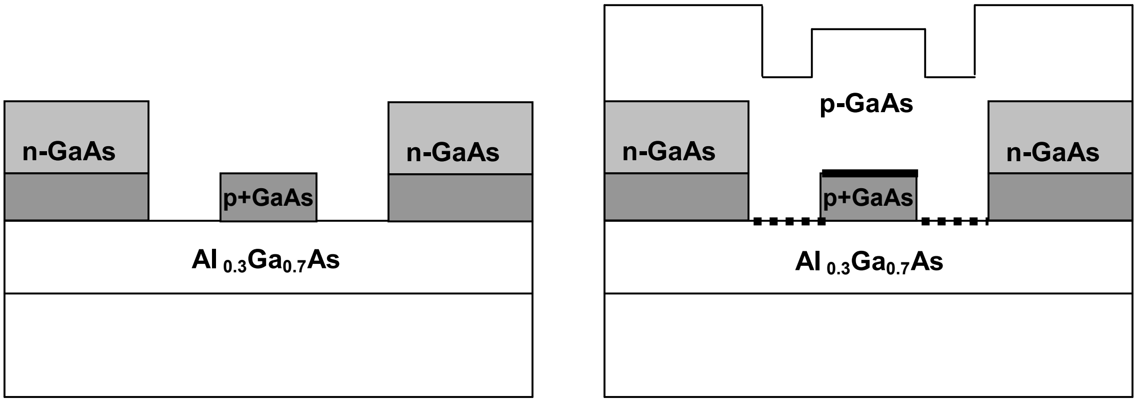

(a)

(b)

Figure 3.2 Schematics of regrowth on different surface causing different Fermi level pinning effect (a) before the regrowth and (b) after the regrowth.

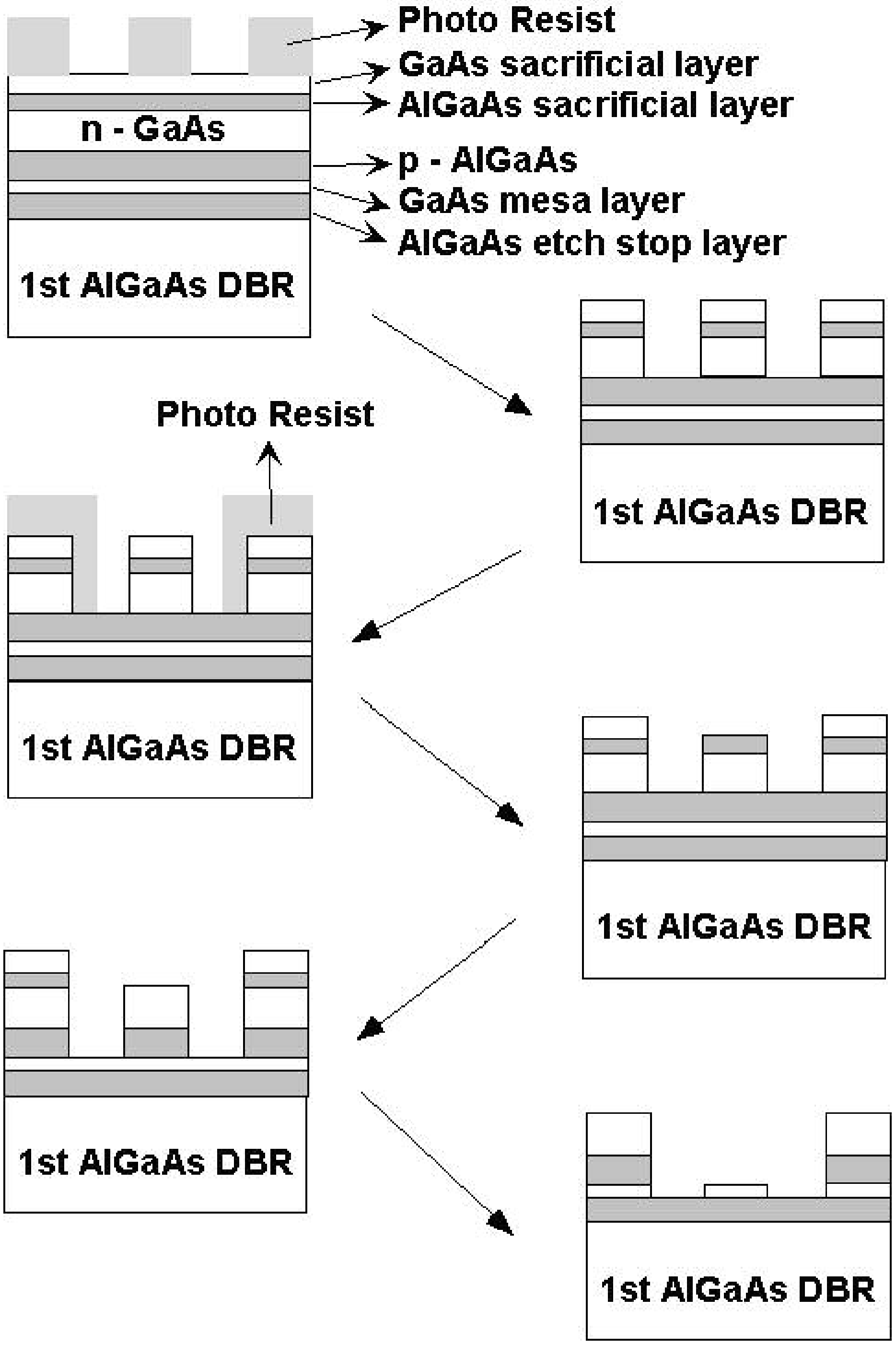

Figure 3.3 Process sequence for fabricating double aperture with intracavity mesa, which includes Fermi level pinning interface.

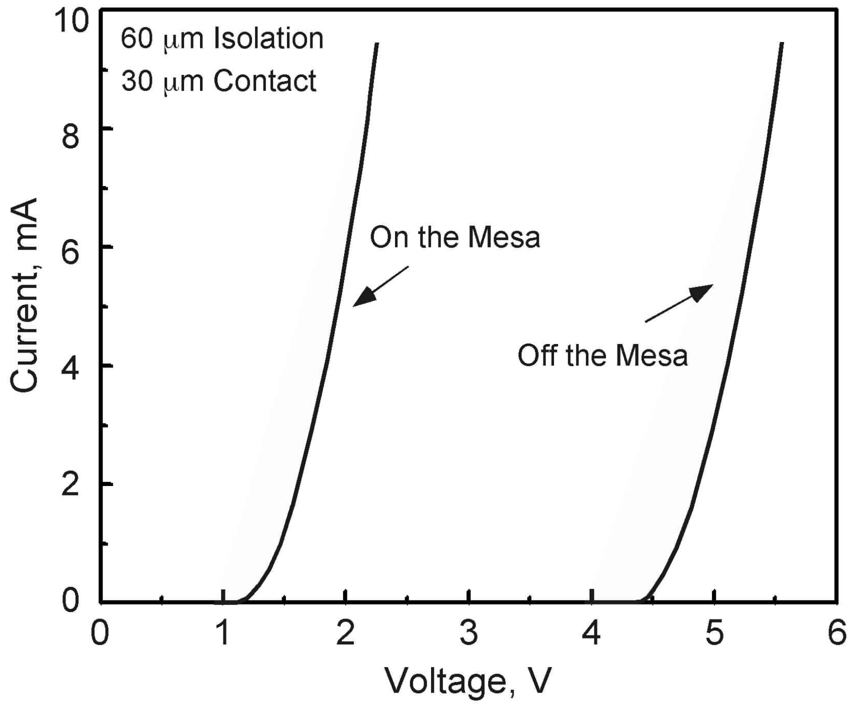

Figure 3.4 I-V characteristics of (a) the all-epitaxial current- and mode-confined VCSEL and (b) the test structure for current confinement on the mesa

3.3 Verification of Self Aligned Mode- and Current Confinement of VCSEL

3.3.1 Design and structure for mode– and current confined VCSEL

The VCSEL cavity consists of 28 lower n-type AlAs/GaAs quarter-wave mirror pairs, an $Al_{0.05}Ga_{0.95}As$ one-wavelength cavity spacer containing three InGaAs/GaAs quantum wells placed at its center, and an upper p-type AlAs/GaAs quarter-wave mirror stack of 18 pairs. The upper mirror stack is rather heavily doped uniformly with C at a level of $5x10^{18}cm^{-3}$ to reduce the electrical resistance, but this also increases the absorption loss of the cavity. The phase-shifting mesa is formed from a single p^+ GaAs layer of 150 Å-thickness, and is placed at the first node of the upper p-type mirror. The epitaxial regrowth that completes the upper mirror starts with GaAs to complete the quarter-wave that forms the first period of the mirror, and then proceeds with the additional 17 p-type AlAs/GaAs mirror periods. A novel feature of this VCSEL is the current confinement to the same lithographically defined phase-shifting mesa. This current confinement is achieved by blocking the current on the back biased p-n junction down to 15 µm-diameter aperture and performing the regrowth outside the phase-shifting mesa of 7 µm-diameter on a p-type $Al_{0.3}Ga_{0.7}As$ crystal surface exposed by removal of the p^+ GaAs layer. Fermi level pinning at the regrown hetero-interface creates the conductivity change between the phase-shifting mesa and its adjoining crystal region, and results in fully self-aligned and lithographically defined fabrication of the all-epitaxial VCSEL.

The process flow for making phase shifting mesa and two different current blocking areas is straightforward as described in the previous section. Starting from the as grown bottom part of VCSELs, the ring opening mask defines two apertures. After selective etching of GaAs/AlGaAs/GaAs, another opening mask defines inner aperture. After etching of GaAs selectively, photo resist is removed and selective etching of AlGaAs/GaAs/AlGaAs is followed. The final structure consists a inner aperture with phase shifting mesa and a outer aperture without the mesa surrounded by the current blocking p-n-p layer.

3.3.2 Optimization of Regrowth Conditions

In contrast to previous regrowth, which is grown on GaAs surface, the morphology of regrown surface is greatly affected by the regrowth conditions due to the different surfaces incorporation on the mesa and ring area of growing atoms. The most prominent feature is abnormal growth at the boundary of mesa. It is believed that the impinging Gallium atoms have preference to adhere on GaAs surface than AlGaAs surface. Therefore with atomic migration on the surface, Gallium atoms can find more favorable sites to grow at the boundary of GaAs mesa. The schematic diagram of this phenomenon is shown in Figure 3.5. This overgrowth should be eliminated for minimizing scattering loss due to abrupt change of electrical field in the boundary.

Low temperature growth of first 30nm of GaAs can solve this problem. At normal growth temperature of 590°C for GaAs gives high enough surface mobility to find most favorable site of GaAs, which might lead the abnormal growth at mesa boundary. As lowering the growth temperature, the surface mobility can be reduced and ad atoms have a tendency to stick on the surface without having a sufficient time move around the surface. Therefore, the growth topology might follow the existing mesa structure. The temperature of 450°C – 500°C range is chosen carefully to ensure the single crystal growth which is required for maintaining optical properties of crystal as grown at normal temperature.

3.3.3 Light Output vs. Current Characteristics

Figure 3.6 shows the light versus current and voltage versus current curves for the 8 μm diameter current- and mode-confined, all-epitaxial VCSEL. Although interface grading is used to reduce the resistance, the doping levels are not optimized for minimum resistance nor low cavity loss [3.4], [3.5]. The p-type C doping of 5×10^{18} cm^{-3} that is used even next to the cavity spacer increases the absorption loss, and increases the threshold current density and decreases the device efficiency [3.5]. Still the threshold current of 1.1 mA, threshold current density of 2.8 kA/cm^2, and differential slope efficiency of 25% for the 7 μm diameter device are comparable to the initial oxide-confined VCSELs that used an upper epitaxial mirror even with optimized C doping profile[3.6], and much lower than for gain-guided VCSELs of comparable device size and wavelength [3.7]. The low threshold and linear light versus current characteristics are indicative of the stable optical mode confinement for VCSELs of this device size [3.7]

3.3.4 Emission Spectrum Analysis

Figure 3.7 shows the below threshold spontaneous emission characteristics from the VCSEL taken at 1 mA bias current. The emission peaked at ~967 nm is from the phase-shifting mesa region, while the emission peaked at ~963 nm is from the region just outside the phase-shifting mesa. The blue shift in emission between the mesa region and the off-mesa region is due to the shift in the vertical cavity resonance that provides the optical mode-confinement. The degree of optical mode-confinement is therefore readily engineered in this type of VCSEL [3.8]. The spectrally integrated intensity of the emission at ~963 nm is 10 times less than that at ~967 nm, indicating that about 90% of the injected current is confined to the phase-shifting mesa.

The good injection efficiency is also evidenced by the lasing behavior of the spectral emission as shown in Figure 3.8. Figure 3.8 shows the lasing spectra between 5 mA and 25 mA. Over the full range of device operation the lasing is obtained only from the mesa region in the spectral range from 968 to 970 nm, with no detected lasing in the spectral range from 963 nm and shorter that would correspond to regions outside the mesa.

3.3.5 Discussions

VCSEL performances are improved using self aligned current confinement of phase shifting mesa by reducing the leakage current around mesa effectively. The regrowth conditions play important roles in controlling device topology and device performance. Regrowth over back biased p-n junction step require more careful investigation on the crystal quality and morphology due to the ambient exposed $Al_{0.7}Ga_{0.3}As$ layer. Generally, single crystal growth over $Al_{0.7}Ga_{0.3}As$ layer can not be achieved without additional in situ treatment of surface due to its higher incorporation of oxygen. In this experiment, I also found some abnormal growth at the sidewall of back biased p-n junction due to the regrowth on $Al_{0.7}Ga_{0.3}As$ layer. This may affect the optical properties of VCSEL by introducing additional scattering. Therefore it is preferable to achieve current confinement without using back biased p-n junction by improving current blocking property of Fermi level pinned GaAs/AlGaAs interfaces. This will make possible to fabricate fully planarized all epitaxial VCSEL without any abnormal crystal deterioration around phase shifting mesa. The next chapter will discuss about this effect.

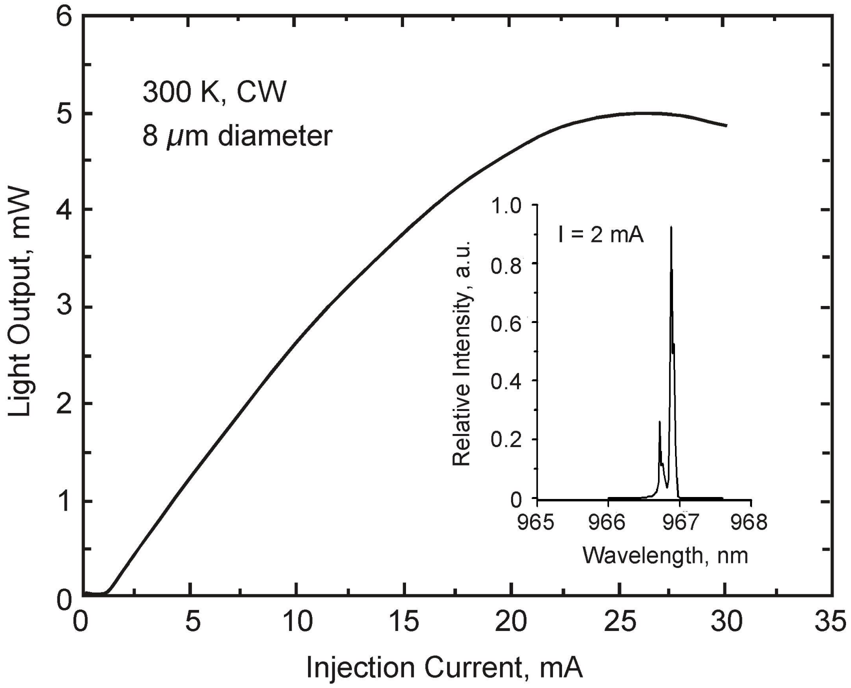

Figure 3.5 Light vs. current characteristics measured for an 8μm diameter, all-epitaxial current- and mode-confined VCSEL. The threshold current is 1mA, the threshold current density is 2kA/cm^2, and the slope efficiency is 25%

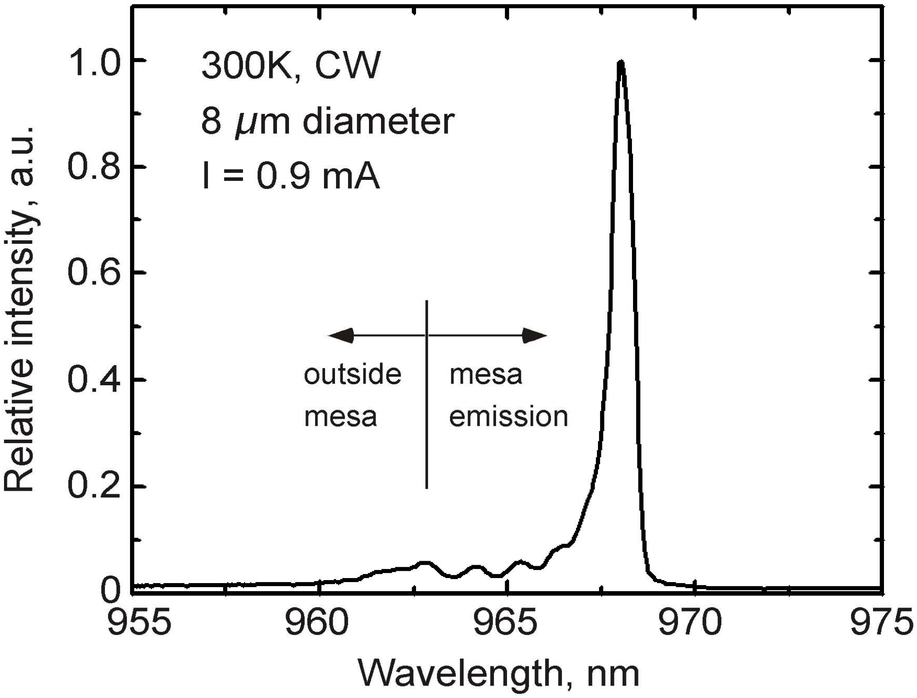

Figure 3.6 Spontaneous spectral emission showing the emission peaked from the mode-confining phase-shifting mesa at 968nm, and the weak spontaneous emission from the region outside the mesa peaked at 963nm. Additional peaks in the spontaneous emission spectra between 968nm and 963nm are transverse cavity modes confined by the 8μm diameter mesa.

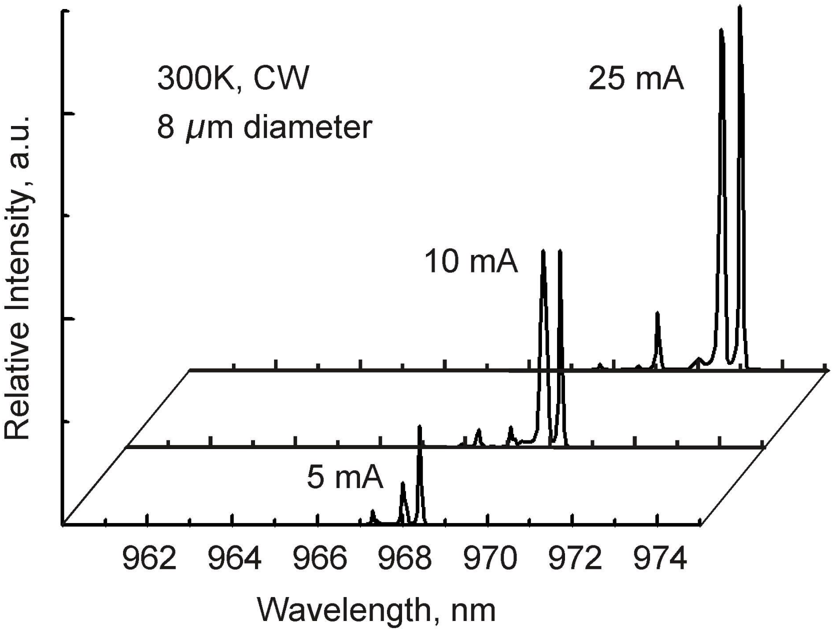

Figure 3.7 Spectral emission above threshold between 5 and 25 mA showing lasing operation only in the wavelength ranges of 968nm over the entire continuous wave operating range of Figure 3.5

3.5 Summary

A novel all-epitaxial current- and mode-confining vertical-cavity surface-emitting laser is demonstrated that eliminates the need for any post-growth oxidation step. The current and optical mode are self-aligned and confined to the same lithographically defined area in an AlGaAs cavity using an epitaxial regrowth. The optical mode-confinement is a key requirement to prevent thermal lensing effects commonly observed in planar implanted VCSELs, while the all-epitaxial and lithographically defined fabrication can extend the VCSEL technology to very high reliability, low thermal impedance, and high yield for dense arrays and new device structures based on intracavity gratings and photonic lattices. Additional improvement of device performance will be possible by eliminating abnormal crystal growth due to $Al_{0.7}Ga_{0.3}As$ in the back bias p-n junction layer.

3.6 References

[3.1] D. Lu, J. Ahn, H. Huang, and D. G. Deppe , "All-epitaxial mode-confined vertical-cavity surface-emitting laser," *Appl. Phys. Lett.,* Vol.85, pp 2169-2171, 2004

[3.2] E.-A Moon and J.-L Lee, " Selective wet etching of GaAs on $Al_xGa_{1-x}As$ for AlGaAs/InGaAs/AlGaAs pseudomorphic high electron mobility transistor," *J. of Appl. Phys.* Vol. 84, pp. 3933-3938, 1998

[3.3] J.-H Kim, D. H. Lim, and G. M. Yang, " Selective etching of AlGaAs/GaAs structure using the solutions of citric acide/H_2O_2 and de-inoized H_2O/buffered oxide etch," *J. Vac. Sci. Technol.*, B 16, pp.558-560, 1998

[3.4] K.L. Lear, R.P. Schneider, K.D. Choquette, S.P. Kilcoyne, J.J. Figiel, and J.C. Zolper, "Vertical cavity surface emitting lasers with 21% efficiency by metalorganic vapor phase epitaxy," *IEEE Photonics Technol. Lett.,* Vol. 6, pp. 1053–1055,1994

[3.5] K.L. Lear, K.D. Choquette, R.P. Schneider, S.P. Kilcoyne, and K.M. Geib, "Selectively oxidized vertical cavity surface emitting lasers with 50% power conversion efficiency," *Electron. Lett.*, Vol. 31, pp. 208–209, 1995

[3.6] K.D. Choquette, R.P. Schneider, K.L. Lear, and K.L. Geib, "Low threshold voltage vertical-cavity lasers fabricated by selective oxidation," *Electron. Lett.*, Vol. 30, pp. 2043–2044, 1994

[3.7] K.L. Lear, R.P.Schneider Jr., K.D. Choquette, and S.P. Kilcoyne, "Index guiding dependent effects in implant and oxide confined verticalcavity lasers," *IEEE Photonics Technol. Lett.*, Vol. 8, pp. 740–742, 1996

[3.8] D.G. Deppe, "VCSELs and quantum dots: state of the art and future directions," *Hot Topics in Photonics 2004, Photonics Europe*, Strasbourg, France, April 1994

Chapter 4. All Epitaxial Mode and Current Confined VCSELs

4.1 Introduction

In this chapter a new lithographically defined approach to form self-aligned index- and current-confined all-epitaxial GaAs-based VCSELs is demonstrate. The new process is based on epitaxial regrowth over an intracavity phase-shifting mesa. The device is illustrated in Fig. 1.2. As I have shown previously, the height of the phase-shifting mesa and its placement in the vertical cavity play important roles in establishing the optical scattering loss due to the mode-confinement [4.1]. The crystal step height should be kept relatively small and is 65 Å in the present devices. The difference between the previous mode- and current confined VCSEL is that back –biased p-n junction is removed for reducing optical scattering by elimination of the abnormal growth at the side wall of $Al_{0.7}Ga_{0.3}As$ which constitute p-n junction. Electrical confinement to the phase-shifting mesa is obtained only by performing the epitaxial growth on different crystal surfaces either on the phase-shifting mesa or on the crystal region outside this mesa to independently control the crystal resistivity in either region.

4.2 Design and Structure of All Epitaxial Mode and Current Confined VCSEL

The VCSEL cavity consists of 28 lower n-type AlAs/GaAs quarter-wave mirror pairs, an $Al_{0.05}Ga_{0.95}As$ one-wavelength cavity spacer containing three InGaAs/GaAs quantum wells placed at its center, and an upper p-type AlAs/GaAs quarter-wave mirror stack of 18 pairs. The upper mirror stack is rather heavily doped uniformly with C at a level of $5x10^{18}$ cm^{-3} to reduce the electrical resistance, but this also increases the absorption loss of the cavity. The phase-shifting mesa is formed from a single p^+ GaAs layer of 65 Å-thickness is placed at the first node of the upper p-type mirror. The epitaxial regrowth that completes the upper mirror starts with GaAs to complete the quarter-wave that forms the first period of the mirror, and then proceeds with the additional 17 p-type AlAs/GaAs mirror periods. A novel feature of this VCSEL is the current confinement to the same lithographically defined phase-shifting mesa. This current confinement is solely achieved by performing the regrowth outside the phase-shifting mesa of 10μm-diameter on a p-type $Al_{0.3}Ga_{0.7}As$ or $Al_{0.4}Ga_{0.6}As$ crystal surface exposed by removal of the p^+ GaAs layer. Fermi level pinning at the regrown interface creates the conductivity change between the phase-shifting mesa and its adjoining crystal region, and results in fully self-aligned and lithographically defined fabrication of the all-epitaxial VCSEL. After finishing crystal growth, ring contact of 30 μm of inner diameter and 60 μm of outer diameter is formed on the p-type upper mirror, the 100 μm of electrical isolation is followed.

4.3 Characterization Results

4.3.1 L-I-V Characteristics

Figure 4.1 shows the light versus current and voltage versus current curves of the VCSEL with $Al_{0.3}Ga_{0.7}As$ etch stop layer and additional test regions fabricated on the VCSEL wafer. The test regions are formed without the phase-shifting mesas and are 100μm-diameter to determine the current versus voltage characteristic that would occur through the current blocking region in the actual VCSEL. The inset of Fig. 4.1 shows the lasing spectrum of the VCSEL at high current. The threshold current is 670 μA, the threshold current density is 863 A/cm^2, and differential slope efficiency is 35%. The VCSEL has a turn on voltage of, 1.2 V and the lasing threshold voltage of 1.4 V.

The intracavity phase-shifting mesa creates a vertical resonance shift of, 10 nm relative to the cavity region outside the mesa. Consistent with the spectral inset in Figure 4.1 taken at 25 mA, I find that lasing occurs only from the 10-μm-diam phase shifting mesa throughout the entire range of currents. Figure 4.1 shows that the all-epitaxial design can be driven to 35 mA before the output power fully saturates, which corresponds to, 50 times threshold. Although I am presently unable to do high temperature testing, the high current characteristics suggest that the current confinement is not overly temperature sensitive.

Despite the current confinement and lasing only from the phase-shifting mesa, Fig. 4.1 shows that the blocking voltage in the region outside the mesa has a reduced turn-on voltage of between 2 and 3 V, which is considerably smaller than the 4.5 V of the test structures. The resistance of the VCSEL is also increased due to the smaller area as compared to the test structures. The smaller turn-on voltage outside the mesa region allows some leakage current around the 10-μm-diam phase-shifting mesa region through the 100 μm etched post.

The ratio of areas between the phase-shifting mesa and 100 μm etched post is approximately 100, and could be readily reduced with additional processing steps to improve the performance. For example, simply using a proton implant would reduce the electrical conductivity well away from the VCSEL active area to force all current into the phase-shifting mesa. In fact, this is highly desirable to reduce the parasitic capacitance and maintain a fully planar, all-epitaxial approach to VCSEL arrays. Optimized interface grading and doping levels would also reduce the electrical resistance, as well as reduce optical loss in the cavity. Both would further reduce the lasing threshold and improve the efficiency [4.2].

4.3.2 Emission Spectrum Analysis

To characterize the electrical confinement in the actual VCSEL device as compared to the test structures, I have evaluated the below threshold spontaneous emission spectrum of the VCSEL looking specifically at emission in the spectral region corresponding to outside the mesa at, 962 nm relative to emission from the mesa in the region of, 972 nm as shown Figure 4.2. These below threshold measurements show that the present VCSELs still exhibit leakage current around the phase-shifting mesa that increases the lasing threshold and decreases efficiency. At the lowest current levels of 40 μA, the integrated intensity of light output from the 100-μm-diam outside mesa region is three times larger than that from the10-μm-diam mesa region, even with the p-metal electrode blocking much of the emission from outside the mesa. As the current is increased the injection into the mesa becomes more efficient and at 150 μA emission from the mesa exceeds that from the outer region. At 500 μA, the emission intensity from the mesa region exceeds that from outside the mesa by a factor of 10, but stimulated emission also contributes to the mesa emission. These results suggest that substantial improvements can still be made in the VCSEL performance based on this lithographic fabrication approach.

$Al_{0.4}Ga_{0.6}As$ layer has larger valence band offset than $Al_{0.3}Ga_{0.7}As$ and would have better blocking of current through the Fermi level pinned $GaAs/Al_{0.4}Ga_{0.6}As$ interface. The same structure with previous VCSEL which have etch stop layer of $Al_{0.3}Ga_{0.7}As$ except for the Al composition of etch stop layer was fabricated and characterized.

Figure 4.3 shows the light versus current and voltage versus current curves of the VCSEL with $Al_{0.4}Ga_{0.6}As$ etch stop layer and additional test regions fabricated on the VCSEL wafer. The threshold current is 1.15 mA, the threshold current density is 1464 A/cm^2, and differential slope efficiency is 44%. The VCSEL has a turn on voltage of, 1.2 V and the lasing threshold voltage of 3.5V. Improved differential efficiency might be resulted from the better current confinement with the $Al_{0.4}Ga_{0.6}As$ etch stop layer, which blocks current up to 3.5 V compare to 1.4 V in

$GaAs/Al_{0.3}Ga_{0.7}As$ interface.

However, threshold current density is increased with $GaAs/Al_{0.4}Ga_{0.6}As$ interface. It is believed due to the surface roughness of current blocking hetero-interface. As increasing Al contents in AlGaAs, the more oxygen in incorporated at the interface between GaAs/AlGaAs junction. The oxygen can be worked as better current blocking barrier but, it may also affect on the surface roughness by changing atomic incorporation rate locally. AFM images is checked on of regrown surface around phase shifting mesa of the VCSELs with $GaAs/Al_{0.3}Ga_{0.7}$ interface and $GaAs/Al_{0.4}Ga_{0.6}$ interface The surface on the mesa region is smooth and ahs roughness value of ~0.5 nm but outside the mesa has rougher surface than on the mesa in both cases. Surface roughness of outside the mesa region with $GaAs/Al_{0.3}Ga_{0.7}$ interface is about ~3 nm while the one with $GaAs/Al_{0.4}Ga_{0.6}$ has ~7 nm. The effect of interface roughness on the optical properties can be analyzed. The next chapter will give some idea how much effect on optical loss.

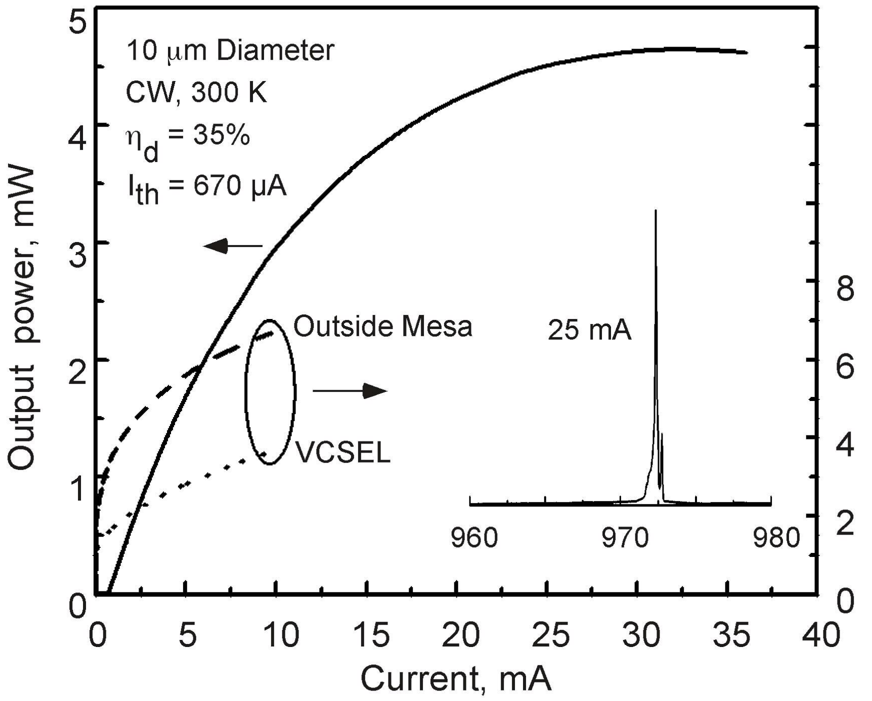

Figure 4.1 Light vs. current characteristics and current vs. voltage characteristics of the all-epitaxial VCSEL with $Al_{0.3}Ga_{0.7}As$ etch stop layer. The inset shows the spectral emission at 25 mA. The lasing at 972 nm corresponds to the phase-shifting mesa region.

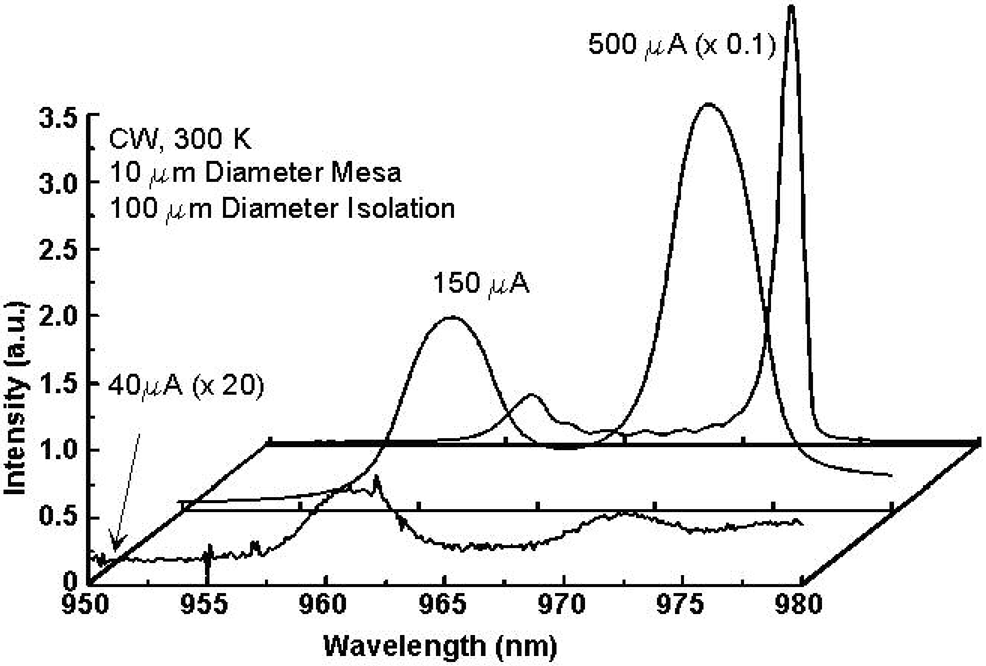

Figure 4.2 Spontaneous emission spectra of the all-epitaxial VCSE at 40μA, 150μA, and 500μA. The relative intensity of light from the outside mesa region to phase shifting mesa region is reducing as increase input current.

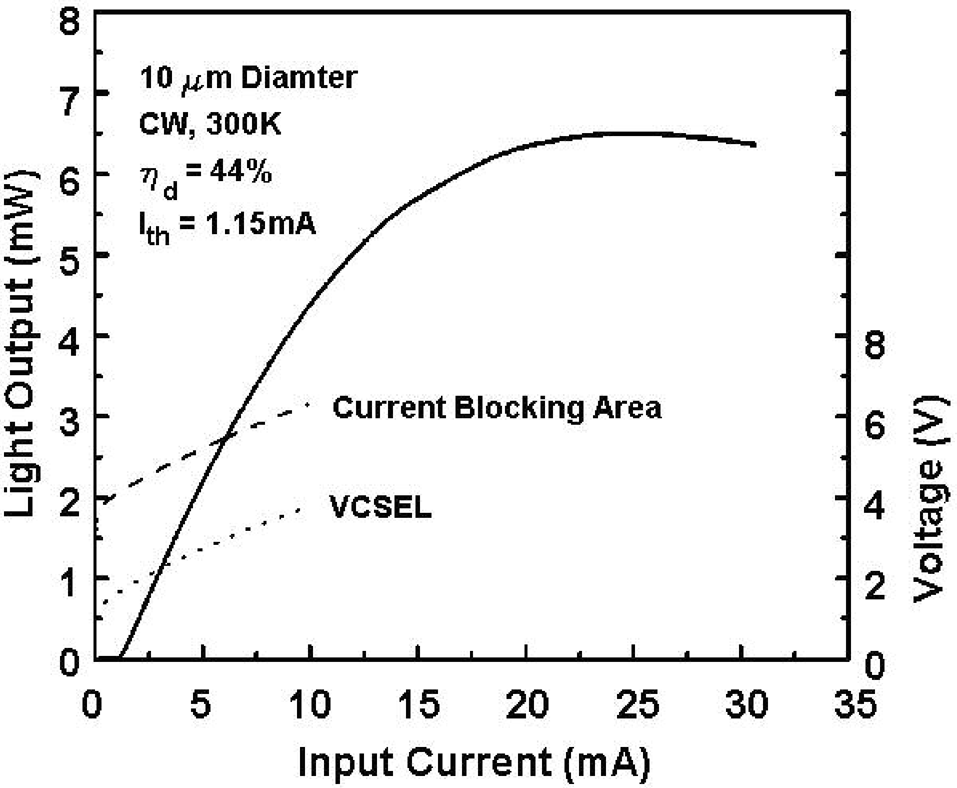

Figure 4.3 Light vs. current characteristics and current vs. voltage characteristics of the all-epitaxial VCSEL with $Al_{0.4}Ga_{0.6}As$ etch stop layer. Turn on voltage outside the mesa is 3.5V.

4.4 Summary

An all-epitaxial current- and mode-confining VCSEL is demonstrated that eliminates the need for any postgrowth oxidation, and can produce fully planar VCSELs and VCSEL arrays. The current and optical mode are self aligned and confined to the same lithographically defined area using an intracavity phase-shifting mesa and selective Fermi level pinning at a buried semiconductor interface. The all-epitaxial and lithographically defined approach can extend the VCSEL technology to very high reliability, low thermal impedance, and high yield for dense arrays and device structures based on intracavity gratings and photonic lattices.

4.5 References

[4.1] D. Lu, J. Ahn, H. Huang, and D. G. Deppe, "All-epitaxial mode-confined vertical-cavity surface-emitting laser," *Appl. Phys. Lett.,* Vol. 85, pp. 2169-2171, 2004

[4.2] J. Ahn, D. Lu, and D. G. Deppe, "All-epitaxial, lithographically defined, current- and mode-confined vertical-cavity surface-emitting laser based on selective interfacial fermi-level pinning," *Appl. Phys. Lett.,* Vol. 86, Art. No. 021106, 2005

[4.3] K. L. Lear, K. D. Choquette, R. P. Schneider, Jr., S. P. Kilcoyne, and K. M. Geib, "Selectively oxidised vertical cavity surface emitting lasers with 50% power conversion efficiency," *Electron. Lett*. Vol. 31, pp. 208-209, 1995

Chapter 5. All Epitaxial Index- and Current Confined Quantum Dot Laser

5.1 Introduction

Since the first quantum dot (QD) laser diode was demonstrated in continuous-wave operation at room temperature [5.1], there have been remarkable improvements in the performance of the QD lasers achieving high power [5.2], long wavelength [5.3], low threshold [5.4], [5.5], and high speed [5.6]. The QD laser presents an interesting change over planar quantum well laser diodes because the active region forms “self-buried” heterostructures. These self-buried heterostructures eliminate or reduce diffusion currents, and yet maintain otherwise planar heterostructures in the active region. Because of the “self-buried” nature of the QD active region, one of the lowest threshold currents has been achieved by a simple double oxide confined structure based on fairly simple fabrication steps [5.5].

Buried heterostructure laser diodes offer superior performance because they can provide simultaneous mode and current confinement. They are used for high power and high-speed laser diodes to obtain single transverse modes. However the fabrication is usually rather complicated, and based on such techniques as impurity-induced layer intermixing or deep etching through the active material and epitaxial regrowth. Both yield and reliability can suffer as a result of these complicated fabrication approaches. As I show below, the QD active material in contrast enables a new approach to fabricate buried-heterostructure laser diodes that offer the potential for very high reproducibility, high yield, good mode control, and high reliability in a fully epitaxial device.

In this chapter I present data to demonstrate a new lithographically defined approach to form self-aligned index- and current-confined all-epitaxial GaAs-based QD lasers. The new process is based on epitaxial regrowth over an intracavity mesa, but with the regrowth occurring above the QD active layers.

5.2 Design and Structure of All Epitaxial Quantum Dot Laser

The device is illustrated in Figure 5.1. The height of the mesa combined with the epitaxial regrowth establishes the index confinement of the optical mode, by presenting an increased effective index in the mesa region. The epitaxial regrowth, though in close proximity, is maintained fully above the QD active material to maintain high crystal integrity in that region. Because the mesa can be kept thin, selective etching can be easily controlled to reproducibly form the lateral size of the mesa. The mesa is ~100 Å in the present devices.

Electrical confinement to the mesa is obtained by a process we call selective Fermi level pinning, which is induced in the region outside the GaAs mesa by regrowth on a low Al content AlGaAs layer. The same AlGaAs layer provides the etch stop that sets the height of the intracavity mesa. The selective Fermi level pinning at the AlGaAs heterointerface confines electrical current only to the GaAs mesa, so that the electrical current and optical mode are self-aligned. In these initial devices additional current confinement layers with back-biased p-n junctions are also used well away from the mode-confining mesa to identify the mesa position and for additional electrical confinement.

Mode confinement to the mesa is achieved by the difference of effective index between the mesa and outside mesa region. When the difference of refractive indices is not too big, the lateral mode profile can be obtained in a similar manner with vertical mode calculation. This is called “weak-guiding model” [5.7]. The effective refractive indices for mesa region and outside mesa region, n_{on} and n_{off}, respectively, can be calculated by solving following equation for each regions.

$$\frac{4\pi d}{\lambda_0}\sqrt{(n_g^2 - n_{eff}^2)} = 4 \cdot \tan^{-1}\left\{ F\sqrt{\frac{n_{eff}^2 - n_c^2}{n_g^2 - n_{eff}^2}} \right\} \tag{5.1}$$

where F is 1 if E-field is TE polarized and F is n_g^2/n_c^2 if E-field is TM polarized, n_g is the refractive index in the cavity, and n_c is the refractive index in the cladding.

An effective index approximation gives an effective refractive index of 3.2217 in the GaAs mesa region, and 3.2175 outside the mesa region. The lateral direction perpendicular to the waveguide, the structure can be approximated as symmetric plana waveguide with guided region with refractive index of 3.2217, and the cladding region with refractive index of 3.2175. Figure 5.2 shows the lateral field profile for 0th mode of 4 μm aperture and 0th and 1st mode of 10 μm aperture. For both aperture widths, the field intensity of 0th mode is negligible at 7.5 μm from the center, whereas the 1st mode extends beyond 7.5 μm form the center.

The QD laser consists of an n-type $Al_{0.7}Ga_{0.3}As$ lower cladding layer, an active region of an undoped $Al_{0.05}Ga_{0.95}As$ and a C-doped $Al_{0.3}Ga_{0.7}As$ waveguide confinement region of thickness of 0.3 μm, with three modulation C-doped InAs QD layers placed at its center, an upper p-type $Al_{0.7}Ga_{0.3}As$ cladding layer, and a p^+ GaAs layer. The active layers are formed from a deposition of 2.5 monolayers of InAs to form a density of 3×10^{10} cm^{-2} QDs per layer with 400 Å GaAs barriers on each side. The upper part waveguide confinement region consists of undoped $Al_{0.05}Ga_{0.95}As$ of thickness of 100 Å and C-doped $Al_{0.3}Ga_{0.7}As$ of thickness of 1000

Å in the aperture region, while the 100 Å thick GaAs mesa is C-doped at $1\text{x}10^{18}$ cm^{-3}.

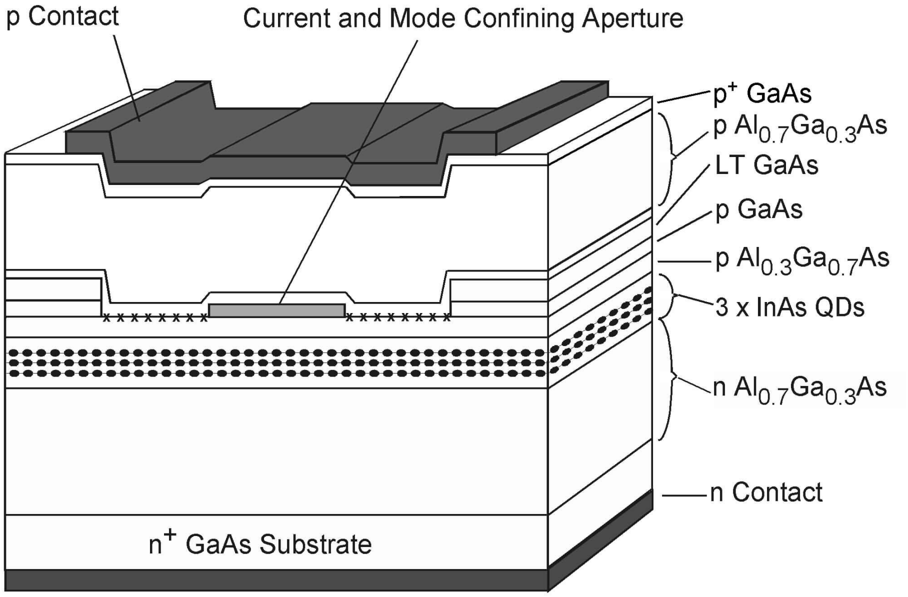

Figure 5.1 Schematic illustration of the all-epitaxial self-aligned current- and mode-confined quantum dot laser that uses an intracavity mesa and selective Fermi level pinning. Selective Fermi level pinning is introduced just above waveguide at the interface shown by the cross-hatch.

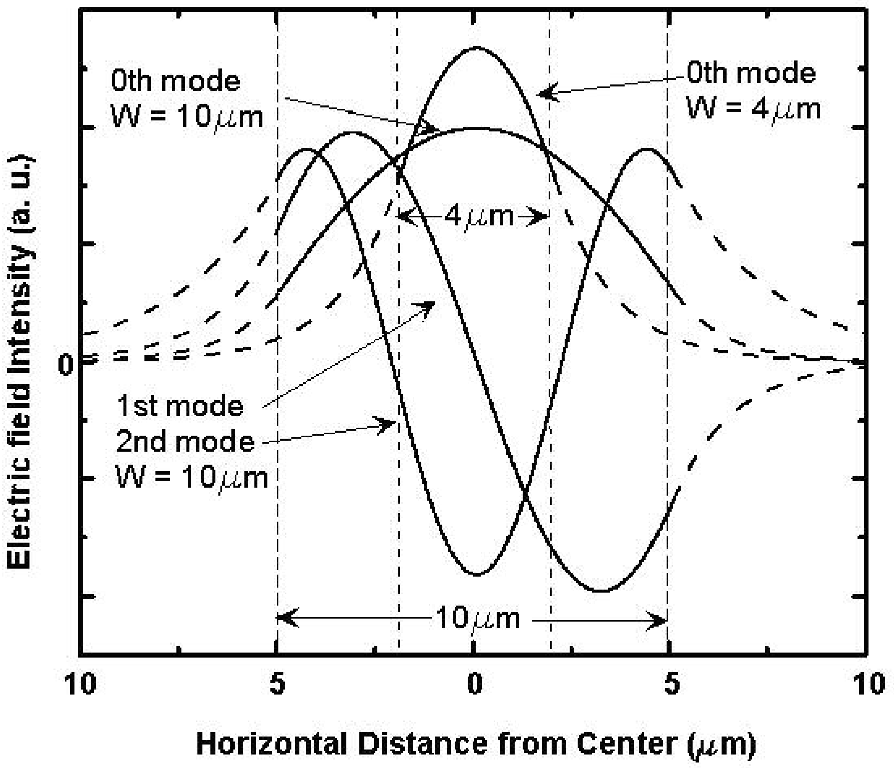

Figure 5.2 Lateral field profiles for 0th mode of 4 μm-wide aperture and 0th, 1st, and 2nd modes for 10 μm-wide apertures

5.3 Experimental Results

5.3.1 I-V Characteristics

In order to characterize the index-guiding aperture, GaAs mesas with three different widths of 4 µm, 6 µm, and 10 µm are defined by selective etching of 100 Å of C-doped GaAs layer stopped on top of $Al_{0.3}Ga_{0.7}As$ waveguide layer. The epitaxial regrowth that completes the upper cladding layer starts with Be-doped GaAs of thickness of 50 Å, and then proceeds with the Be-doped $Al_{0.7}Ga_{0.3}As$ cladding layer. Fermi level pinning at the regrown AlGaAs/GaAs heterointerface creates the conductivity change between the phase-shifting mesa and its adjoining crystal region, and results in fully self-aligned and lithographically defined fabrication of the current- and mode-confined all-epitaxial QD laser.

Figure 5.3 shows the current vs. voltage characteristics measured either through (a) the QD laser that contains an intracavity GaAs mesa of 6 µm x 2 mm and the region outside the ridge of width of 4.5 µm in each side, or (b) an isolated mesa formed from the region outside the ridge containing the AlGaAs/GaAs regrown heterojunction with diameter of 20 µm. The measurements show that the forward voltage for easy current flow is increased from ~1.1 V in the QD laser to >5 V in the electrically confining region that contains the AlGaAs/GaAs heterointerface with selective pinned Fermi level. Therefore the electrical current injected into the device flows only through the intracavity GaAs mesa.

5.3.2 Lasing Spectrum and L-I Characteristics

Spectral measurements for different stripe widths show that ground state lasing at a wavelength of ~1.25 µm occurs for all devices in Figure 5.4. Figure 5.5 shows room temperature characteristics of the light versus current for the 1 mm length as cleaved QD lasers with different widths in pulsed operation mounted p-up on copper heat sinks, and no thinning of the ~500 µm substrate is used. The inset shows the thresholds for different laser widths. The threshold currents for the 1 mm long cavities are ~21 mA for the 4 µm width, 24 mA for the 6 µm width, and 29 mA for the 10 µm width, giving threshold current densities of 446 A/cm^2, 388 A/cm^2, and 295 A/cm^2, respectively. These threshold current densities are higher than for other QD lasers that use similar active regions from our laboratory [5.8]. However, these lasers are robust, and operate up to our maximum possible drive currents of 1.5 A of the pulse generator. This robust operation is quite different than the oxide-confined QD lasers we demonstrated previously, and comes from the all-epitaxial design that is free of internal device strain. These measurements indicate that with optimized heat sinking and fabrications, this approach can produce robust QD lasers.

5.3.3 Waveguide loss Analysis

Figure 5.6 shows the measurements of the inverse differential quantum efficiency versus cavity length for the different mesa widths to analyze the waveguide losses. The waveguide losses are extracted from the laser cavity lengths of 2 and 3 mm, while gain saturation influences the operating characteristics at the shorter cavities as shown in Fig. 5.6. The slopes of the inverse differential quantum efficiency versus cavity length give a constant internal efficiency of 75% for each of the QD laser stripe widths. These results also show a consistent increase of waveguide loss from 8.14 cm^{-1} to 10.22 cm^{-1} with decreasing widths from 10 to 4 μm. Internal losses of QD lasers with similar active regions show waveguide losses of from 2 to 4 cm^{-1}, so that the additional 6 to 8 cm^{-1} waveguide loss in the present devices is due to the epitaxial regrowth. As discussed above, our other experiments of epitaxial regrowth on AlGaAs suggest that this loss can be substantially reduced for optimized regrowth conditions, such as increasing the GaAs deposition in the initial regrowth to fully smooth the growth surface.

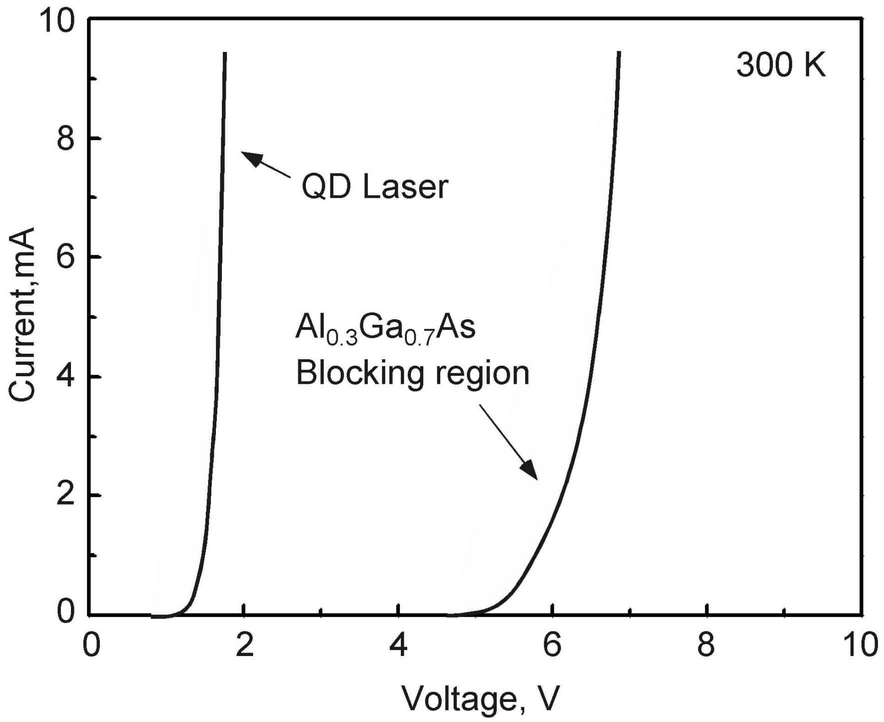

Figure 5.3 Current vs. voltage characteristics through 6 μm x 2.19 mm of all-epitaxial QD lasers and current blocking region with 20 μm of diameter post. The curves correspond to either through the whole device with intracavity mesa, blocking region, and reverse p-n junction (QD laser) or through an interface containing the Fermi level pinning (AlGaAs blocking region).

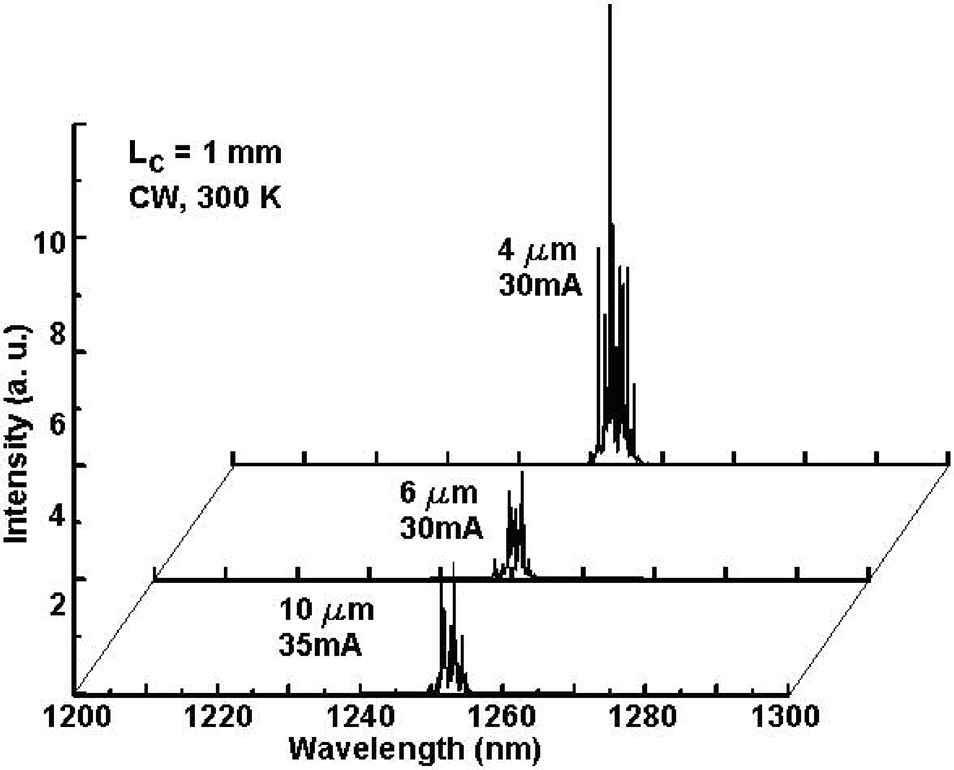

Figure 5.4 Lasing Spectra of the all-epitaxial QD lasers with different width of 4 μm, 6 μm, and 10 μm. All lasers show ground state lasing centered wavelength of 1.25μm.

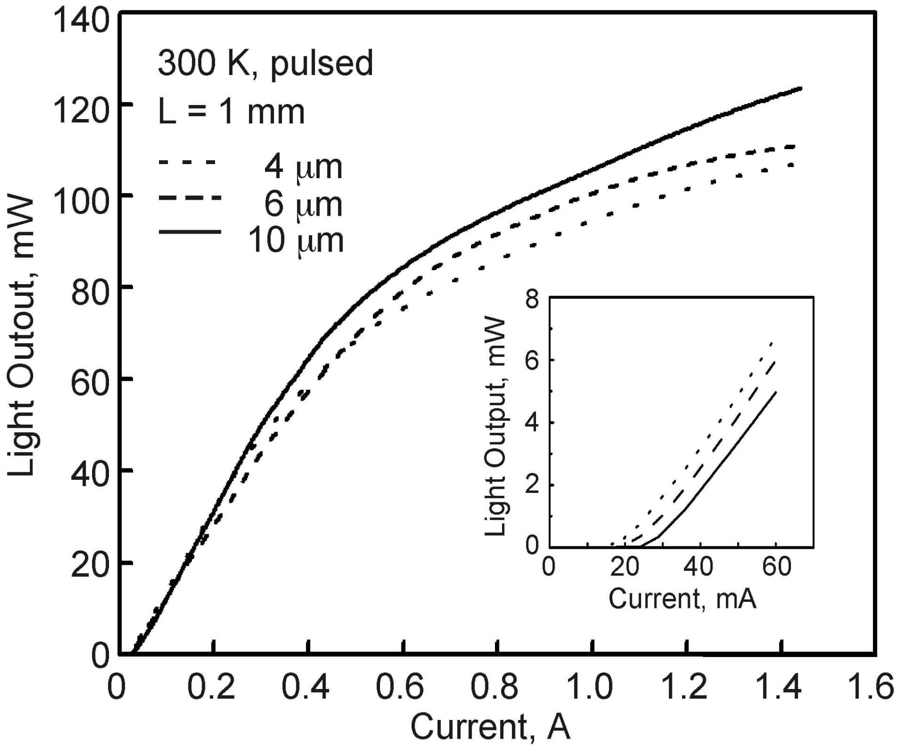

Figure 5.5 Light vs. current characteristics of the all-epitaxial QD lasers with different width of 4 μm, 6 μm, and 10 μm. The inset shows the threshold behavior

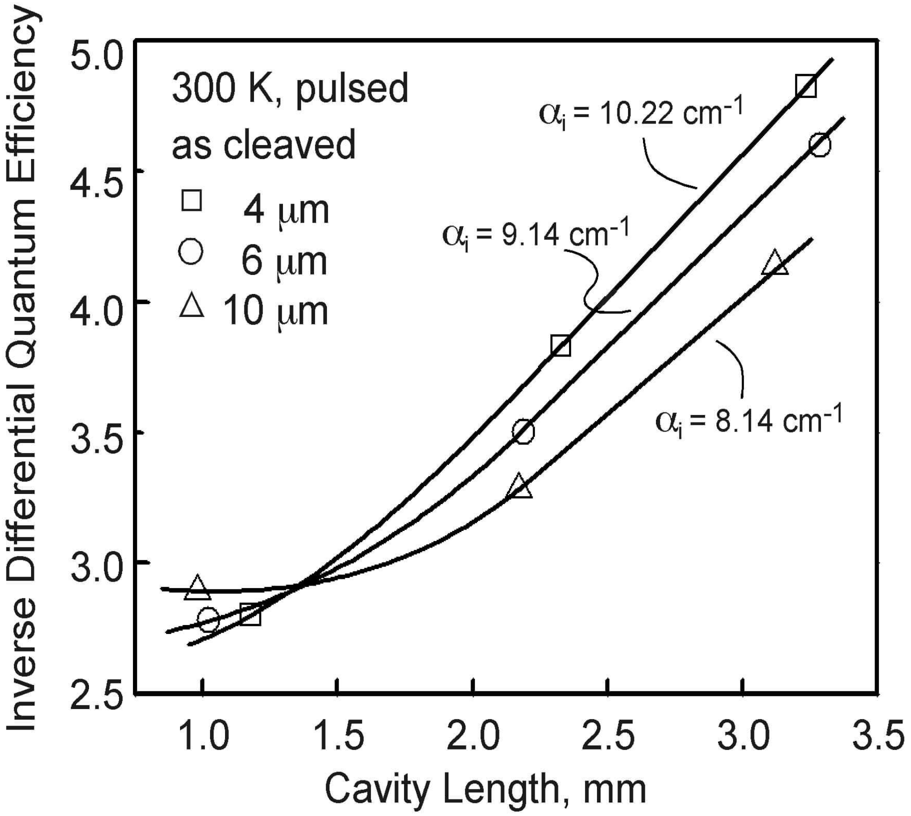

Figure 5.6 Inverse of differential quantum efficiency versus cavity length of all-epitaxial QD lasers with different aperture widths of 4 μm, 6 μm, and 10 μm. The trend lines fit on the data for two longer cavity lengths of each device and give internal waveguide losses of 10.22, 9.14, and 8.14 cm^{-1}, respectively.

5.4. Discussions

I have performed numerous regrowths of GaAs on AlGaAs to study the impact of growth parameters on surface morphology. I find that for $Al_xGa_{1-x}As$ compositions with $x \leq 0.4$ excellent surface morphology can be obtained when GaAs is first deposited in the regrowth to smooth the crystal surface. Generally, the amount of GaAs needed for surface smoothing is > 400 Å. In the QD lasers described below a large index step is created between the GaAs mesa and outside region by using only a thin GaAs deposition of 50 Å over the GaAs mesa. Examination of the surface morphology under an optical microscope shows that a slight surface roughening occurs outside the mesa region for the GaAs regrowth on AlGaAs, while the regrowth on the GaAs mesa region appears smooth. As described below, this surface roughening leads to an increase in the optical waveguide loss. We believe this excess waveguide loss can be substantially reduced and perhaps fully eliminated with optimized regrowth.

The potential of this process to create a highly reliable, robust, and high power QD laser technology is considerable. Excellent uniformity is possible because of the lithographically defined, self-aligned mode- and current-confined self-buried heterostructure. In addition, the etching is highly reproducible because of the width-to-height aspect ratio of the intracavity GaAs mesa, and the excellent etch stop on AlGaAs. The extension to highly uniform index-confined arrays is therefore straightforward, while the all-epitaxial and nearly planar device structure can lead to robust, highly reliable devices. Moreover, the self-aligned mode- and current-confined can be arbitrarily patterned, for example to introduce tapers, y-joints, multi-mode interference filters, or even intracavity gratings. This all-epitaxial approach may also be of interest for high speed through its combination with proton implantation to reduce parasitic capacitance.

5.5 Summary

I demonstrate a new type of laser diode that uses selective Fermi-level pinning at a heterointerface to obtain lithographically defined, self-aligned current- and mode-confinement. When combined with the QD active material that forms “self-buried” heterostructures, the new device approach can lead to robust, highly uniform nearly planar buried heterostructure laser diodes that are easily combined into arrays for high power. Optimized growth conditions can lead to very low optical loss, and high efficiency. This new type of laser diode is promising for enhanced transverse and longitudinal mode control because it increases the potential for arbitrary patterning of the mode-confinement and current injection.

5.6 References

[5.1] N. Kirstaedter, N. N. Ledentsov, M. Grundmann, D. Bimberg, V. M. Ustinov, S. S. Ruvimov, M. V. Maximov, P. S. Kop'ev, Zh. I. Alferov, U. Richter, P. Werner, U. Gosele, and J. Heydenreich, "Low threshold, large T_o injection laser emission from (InGa)As quantum dots," *Electron. Lett.* Vol. 30, pp. 1416, 1994

[5.2] A.R. Kovsh, A.E. Zhukov, N.A. Maleev, S.S. Mikhrin, D.A. Livshits, Y.M. Shernyakov, M.V. Maximov, N.A. Pihtin, I.S. Tarasov, V.M. Ustinov, Z.I. Alferov, J.S. Wang, L. Wei, G. Lin, J.Y. Chi, N.N. Ledentsov, and D. Bimberg, "High power lasers based on submonolayer InAs-GaAs quantum dots and InGaAs quantum wells," *Microelectron. J.* Vol. 34, 491, 2003

[5.3] D.L. Huffaker, G. Park, Z. Zou, O.B. Shchekin, and D.G. Deppe, "1.3µm room-temperature GaAs-based quantum-dot laser," *Appl. Phys. Lett.* Vol. 73, pp. 2564-2566, 1998

[5.4] G.T. Liu, A. Stintz, H. Li, K.J. Malloy, and L.F. Lester, "Extremely low room-temperature threshold current density diode lasers using InAs dots in $In_{0.15}Ga_{0.85}As$ quantum well," *Electron. Lett*, V ol. 35, pp. 1163-1164, 1999

[5.5] G. Park, O.B. Shchekin, D.L. Huffaker, and D.G. Deppe, "Low-threshold oxide-confined 1.3-µm quantum-dot laser," *IEEE Phot. Tech. Lett.* Vol. 12, pp. 230-232, 2000

[5.6] S. Ghosh, S. Pradhan, and P. Bhattacharya, "Dynamic characteristics of high-speed In0.4Ga0.6As/GaAs self-organized quantum dot lasers at room temperature," *Appl. Phys. Lett.* Vol. 81, pp. 3053-3055, 2002

[5.7] A. B. Buckman, "Guided-Wave Photonics," *Saunders College Publishing,* Chap. 2, 1992

[5.8] O.B. Shchekin and D.G. Deppe, "Low-threshold high-T_0 1.3-µm InAs quantum-dot lasers due to p-type modulation doping of the active region," *IEEE Phot. Tech. Lett.,* Vol. 14, pp. 1231-1233, 2002

Chapter 6. Conclusion

The most important aspect of all epitaxial VCSELs is that the patterning of the aperture can be done with lithographic definition. Therefore, the shape, size and density of the aperture are totally arbitrary so that the optical mode is capable of being controlled in a highly sophisticated manner in order to obtain advanced optical characteristics of VCSELs that cannot be achieved with conventional structures.

All-epitaxial current- and mode-confined VCSELs demonstrated in this work have inherent advantages over the previous structures. Selective shallow etching on the intracavity permits the defining of very small feature size and high density of arrays. The intracavity phase-shifting mesa, which is very close to the cavity where the region with the electric field is located, creates a relatively strong impact on the effective cavity length so that the transverse wave vector selection can be achieved even with a small step. This is important to keep the scattering loss low at the step.

The mode confinement and self-aligned current-confinement created by an intracavity phase-shifting mesa has been verified by the VCSELs designed for each purpose. A precisely controlled thin phase-shifting mesa eliminates diffraction loss by cutting off the lateral electric field outside the mesa region while maintaining a low scattering loss due to the step height. Fermi-level pinning at the regrown hetero-interfaces are utilized to confine the current by effectively blocking the current.

All epitaxial, fully planarized mode- and current confined VCSELs, which have only a single phase shifting mesa and which surround current blocking regions, are successfully demonstrated with considerably improved efficiency and threshold current density. The all-epitaxial and lithographically defined approach can extend the VCSEL technology to very high reliability, low thermal impedance, and high yield for dense arrays and device structures based on intracavity gratings and photonic lattices.

An all epitaxial index and current confined quantum dot laser is also successfully demonstrated by showing the ground state lasing and stable operation at a higher input current. This new type of laser diode is promising for enhanced transverse and longitudinal mode control because it increases the potential for arbitrary patterning of the mode-confinement and current injection.

The performances of VCSELs and QD lasers presented in this work can be improved by optimization of the regrowth condition and device engineering of electrical resistance and optical loss. Extensive work on *in situ* treatment of the hydrogen atom on the surface is underway to reduce optical scattering due to the interfaces roughness and sidewall abnormal growth while maintaining good electrical confinement. Device engineering is also underway to maximize wall plug efficiency by reducing electrical resistance and free carrier absorption in the DBRs for high power application. In conclusion, the all epitaxial approach will be one of the crucial technologies for the next generation of VCSEL and edge emitting lasers.

Bibliography

B. J. Thibeault, T. A. Strand, T. Wipiejewski, M. G. Peters, D. B. Young, S. W. Corzine, L. A. Coldren, and J. W. Scott, “Evaluating the effect of optical and carrier lossed in etched post vertical cavity lasers”, *J. Appl. Phys.* Vol.78, pp. 5871-5875, 1995

K. L. Lear, R. P. Schneider, Jr. K. D. Choquette, and S. P. Kilcoyne, “ Index guiding effects in implant and oxide confined vertical-cavity lasers”, *IEEE Photon. Technol. Lett.*, vol. 8, pp. 740-721, 1996

N. Holonyak, Jr., and J. M. Dallesasse, USA Patent #5,262,360 , 1993

S. Guha, F. Agahi, B. Pezeshki, J. A. Kash, D. W. Kisker, and N. A. Bojarczuk, “Microstructure of AlGaAs-oxide heterolayers formed by wet oxidation”, *Appl. Phys. Lett.*, vol. 68, pp. 906-908, 1996

A. C. Alonzo, X. C. Cheng, and T. C. McGill, “ Strain in wet thermally oxidized square and circular mesas” *J. Appl. Phys.* Vol.87, pp. 4594-4599, 2000

J. P. Landesman, A. Fiore, J. Nagle, V. Berger, E. Rosencher, and P. Puech, “ Local stress measurements in laterally oxidized GaAs/AlGaAs heterostructures by micro-Raman spectroscopy’, *Appl. Phys. Lett.*, vol. 71, pp. 2520-2522, 1996

L.M.F. Chirovsky, W.S. Hobson, R.E. Leibenguth, S.P. Hui, J. Lopata, G.J. Zydik, G.
Giaretta, K.W. Goosen, J.D. Wynn, A.V. Krishnamoorthy, B.J. Tseng, J.M. Vandenberg, and L.A. D’Asaro, “Implant-apertured and index-guided vertical-cavity surface-emitting lasers (I2-VCSELs),” *IEEE Phot. Tech. Lett.*, vol. 11, pp. 500-502, 1999

M. Ortsiefer, R. Shau, G. Bohm, F. Kohler, and M.-C. Amann, “Low-threshold index guided 1.5 μm long-wavelength vertical-cavity surface-emitting laser with high efficiency,” *Appl. Phys. Lett.*, vol. 76, pp. 2179-2181, 2000

D.G. Deppe, “VCSELs and quantum dots: State of the art and future directions,”*Hot Topics in Photonics 2004, Photonics Europe*, April 26-30, Strasbourg, France, 1994

D. G. Deppe, T, -H, Oh, and D. L. Huffacker, “Eigenmode confinement in the dielectrically apertured Fabry-Perot microcavity”, *IEEE Phot. Tech. Lett.*, vol. 9, pp. 713-715, 1997

K.L. Lear, R.P. Schneider, K.D. Choquette, S.P. Kilcoyne, J.J. Figiel, and J.C. Zolper, “Vertical cavity surface emitting lasers with 21% efficiency by metalorganic vapor phase epitaxy,” *IEEE Phot. Tech. Lett*., vol. 6, pp. 1053-1055, 1994

K.L. Lear, K.D. Choquette, R.P. Schneider, Jr., S.P. Kilcoyne, and K.M. Geib, “Selectively oxidized vertical cavity surface emitting lasers with 50% power conversion efficiency,” *Electron. Lett*., vol. 31, pp. 208-209, 1995

K.D. Choquette, R.P. Schneider, Jr., K.L. Lear, and K.M Geib, “Low threshold voltage vertical-cavity lasers fabricated by selective oxidation,” *Electron. Lett*., vol. 30, pp. 2043-2044, 1994

N. Kirstaedter, N. N. Ledentsov, M. Grundmann, D. Bimberg, V. M. Ustinov, S. S. Ruvimov, M. V. Maximov, P. S. Kop'ev, Zh. I. Alferov, U. Richter, P. Werner, U. Gosele, and J. Heydenreich, **“**Low threshold, large T_0 injection laser emission from (InGa)As quantum dots”, *Electron. Lett.* **30**, 1416 (1994).

A.R. Kovsh, A.E. Zhukov, N.A. Maleev, S.S. Mikhrin, D.A. Livshits, Y.M. Shernyakov, M.V. Maximov, N.A. Pihtin, I.S. Tarasov, V.M. Ustinov, Z.I. Alferov, J.S. Wang, L. Wei, G. Lin, J.Y. Chi, N.N. Ledentsov, and D. Bimberg, “High power lasers based on submonolayer InAs-GaAs quantum dots and InGaAs quantum wells”, *Microelectron. J.* vol. 34, 491, 2003

D.L. Huffaker, G. Park, Z. Zou, O.B. Shchekin, and D.G. Deppe, “1.3μm room-temperature GaAs-based quantum-dot laser”, *Appl. Phys. Lett.* vol. 73, pp. 2564-2566, 1998

G.T. Liu, A. Stintz, H. Li, K.J. Malloy, and L.F. Lester, **“**Extremely low room-temperature threshold current density diode lasers using InAs dots in $In_{0.15}Ga_{0.85}As$ quantum well”*, Electron. Lett*., vol. 35, pp. 1163-1164, 1999

G. Park, O.B. Shchekin, D.L. Huffaker, and D.G. Deppe**, “**Low-threshold oxide-confined 1.3-μm quantum-dot laser”, *IEEE Phot. Tech. Lett.* vol. 12, pp. 230-232, 2000

S. Ghosh, S. Pradhan, and P. Bhattacharya, “Dynamic characteristics of high-speed In0.4Ga0.6As/GaAs self-organized quantum dot lasers at room temperature”, *Appl. Phys. Lett.* vol. 81, pp. 3053-3055, 2002

O.B. Shchekin and D.G. Deppe, “ Low-threshold high-T_0 1.3-μm InAs quantum-dot lasers due to p-type modulation doping of the active region”, *IEEE. Phot. Tech. Lett* vol. 14, pp. 1231-1233, 2002

E.-A Moon and J.-L Lee, “ Selective wet etching of GaAs on $Al_xGa_{1-x}As$ for AlGaAs/InGaAs/AlGaAs pseudomorphic high electron mobility transistor”, *J. of Appl. Phys.* Vol. 84, pp. 3933-3938, 1998

J.-H Kim, D. H. Lim, and G. M. Yang, “ Selective etching of AlGaAs/GaAs structure using the solutions of citric acide/H_2O_2 and de-inoized H_2O/buffered oxide etch”*, J. Vac. Sci. Technol.*, B 16, pp.558-560, 1998

Vita

Jaemin Ahn was born in Pusan, Korea, on November 2, 1969, the son of Kwangmo Ahn and Yongsoon Jung. He graduated from Kyoungnam High School in Pusan, Korea and entered Hanyang University in Seoul, Korea in 1987. He received his bachelor's and master's of science degrees in inorganic material engineering from Hanyang University in Seoul, Korea, in 1991 and 1994, respectively. In 1994, he joined the Research and Development Center of Varian Korea Ltd. in Pyoungtaek, Korea. In 1997, he moved to the Memory Research and Development Division of Hynix Semiconductor in Ichon, Korea. He worked as a process and device engineer and participated in the development of several state-of-the-art DRAM products at Hynix. In August 2001, he started his Ph.D. studies in the Department of Electrical and Computer engineering at The University of Texas at Austin.

Permanent address: 1082-12, Koejung 4 Dong, Saha Gu, Busan City, Republic of Korea, 603-084

This dissertation was typed by the author.